Archives of Materials Science and Engineering

Volume 58
Issue 2
December 2012
Pages 80-109

International Scientific Journal
published monthly by the
World Academy of Materials
and Manufacturing Engineering

Magnetism in disordered materials

A. Chrobak*
Augut Chełkowski Institute of Physics, University of Silesia,
ul. Uniwersytecka 4, 40-007 Katowice, Poland
* Corresponding e-mail address: artur.chrobak@us.edu.pl

Received 15.10.2012; published in revised form 01.12.2012

ABSTRACT

Purpose: The paper is a review of some problems concerning micromagnetism and magnetism in disordered system.Magnetism of disordered systems is an important problem in analysis of many magnetic materials. As we understand, the term disorder is associated with the both structural (topological and/or chemical) and magnetic (interactions, anisotropy) failures. Typical materials, where phenomena are influenced by the disorder are amorphous and nanocrystalline alloys, nanostructures of magnetic objects, nanoconposites, diluted magnetic materials and intermetallic compounds of rare earth and transition metals. Moreover, in polycrystalline samples can be observed some anomalies related to the area between the grains, which inherently carries some attributes of the disorder. Thus, knowledge of the subject presented here is essential for the proper analysis of magnetics with elements of disorder. In the paper the following problems are discussed: i)magnetization processes in nanosized objects including the famous Stoner-Wohlfarth model, ii) superparamagnetism and magnetic viscosity (time dependent effects), iii) random field Ising model, random bond model and random anisotropy model. Applications of the theories for selected materials (magnetically soft and hard, thin layers, diluted magnetics, and powder systems) are also shown.

Design/methodology/approach: Magnetism in disordered materials is a complex problem that, until now, has not exact solutions. There the two approaches. One of them requires some approximation of the problem in order to obtain exact analytical results. The second approach consists in numerical analysis of exact problem that leads to approximated solutions. In the both cases it is important in which stage of a model the disorder is introduced. In the paper the two approaches are widely discussed.

Findings: The main conclusion of the paper is that some unusual magnetic properties can be attributed to magnetic and structural disorder.

Practical implications: Application of the presented in the paper models indicate that in many magnetic materials the contribution of magnetic disorder plays an important role and should be taken onto account in order to perform correct analysis.

Originality/value: The presented collection of different theoretical models including some elements of micromagnetism and magnetism in disordered system as well as applications of the theories to modern magnetric materials is an original idea. The paper is addressed to scientists and researchers that deal with magnetism and related subjects.

Keywords: Magnetism; Disordered systems; Amorphous and nanocrystalline alloys; Langevin granulometry

Reference to this paper should be given in the following way:

A. Chrobak, Magnetism in disordered materials, Archives of Materials Science and Engineering 58/2 (2012) 80-109.

RESEARCH MONOGRAPH

1. Introduction

A progress of modern technologies requires novel materials with properties that can be optimize for different applications. In many areas it is necessary to use materials with broad spectrum of magnetic properties. Development of electro-energetics, electronics or even computer science would not be possible without externally soft or hard magnets. From this point of view during last few decades one can observe an increasing interest of amorphous alloys, nanocrystalline alloys and nanocomposites [1]. It is well known that by a proper chemical composition and magnetic nanostructure (magnetic nanograins embedded into magnetic/nonmagnetic matrix) one can control different magnetic properties such as the Curie temperature, permeability, coercivity, saturation magnetization, remanence, magnetocaloric effect etc. In other words, almost all magnetic properties of nanostructured materials depend on size of nanograins, their composition and distribution. One can mention two characteristic effects i.e. the so-called enhancement of soft magnetic properties and magnetic hardening, both caused by a specific system of magnetic nano-objects and their interactions. For example, relative magnetic permeability of nanostructered iron-base alloys reaches the value of 10^5-10^6 which is about 1000 times higher than for conventional soft magnets. From the opposite site, it is also known that a certain nanostructure of magnetically hard compounds can lead to further significant magnetic hardening - like for Fe-B-Nd sintered permanent magnets [2]. The key for understanding the mention above effects is magnetic disorder introduced by different agents such as fast cooling from liquid phase (chemical and topological disorder [3]), deformation, nanostructure or magnetic frustrations. One can say that the disorder can be connected with some fluctuations of interatomic distances and nearest surroundings at atomic level as well as with some fluctuation of characteristic magnetic properties (e.g. magnetocrystalline anisotropy, easy magnetization axis …) at cluster or nanograins level. In this situation one can expect some deviations of exchange interactions between atomic magnetic moments which results in a change of magnetic behaviour of the material. Fully amorphous alloys and in the so-called relaxed amorphous state show atomic disorder (chemical and/or topological) per definition and are good examples of materials that the disorder affects their properties. In the case of nanostructures possible magnetic interactions can introduce some new factors leading to an appearance of a new quantity different from the system of separated nanograins. Very interesting are composites that contain coupled (in atomic level) different magnetic phases with different properties (e.g. soft and hard). A specific balance between content of the phases and magnetic disorder can significant enhance hard magnetic properties of such materials. Apart from that, in many other polycrystalline alloys or compounds some unusual behaviours, originated from intergrain regions that possess some attributes of crystal and magnetic disorder, can be observed.

Magnetism in disordered materials is a complex problem. In general, there the two approaches. One of them requires some approximation of the considered problem in order to obtain exact analytical results. The second approach consists in numerical analysis of exact problem that leads to approximated solutions. In the both cases it is important in which stage of a model the disorder is introduced. One can list three main models usually applied in practice i.e. random field Ising model (RFIM), random bond (RB) and random anisotropy (RA) that include magnetic disorder in molecular field, exchange integral and direction of easy magnetization axis, respectively. The common way of the models is to define global free energy of the considered system that includes i) energy of interactions between magnetic moments, ii) interactions between external magnetic field and magnetic moments as well as iii) energy of magnetic anisotropy. All of these factors can contain some fluctuations attributed to a disorder. The free energy depends on the introduced disorder and some magnetic parameters such as external magnetic field, magnetization, directions of magnetic moments, the so-called order parameter (see next section). It can be optimized in order to find a minimum with regards to the parameters that leads to final results. It is worth to notice that in a case of low-dimensional objects an important role plays also shape and surface anisotropies as well as specific interactions between the objects.

The question, which model should be taken into account for a specific problem has not a good answer. It depends on a kind of disorder that is dominant in the analysed system. This is the reason why the knowledge of the mentioned models is very helpful in characterization of real magnetic materials with contribution of structural and/or magnetic disorder. The models are usually tested by a comparison with experimental magnetic characteristics such as thermomagnetic curves, magnetic isotherms, hysteresis loops and the so-called zero field cooled - field cooled (ZFC-FC) curves.

The aim of this review is to summarize models of magnetism in low dimensional objects and disordered systems. In Section 2, problems of magnetization processes in nanosized objects including the famous Stoner-Wolfarth model, superparamagnetism and magnetic viscosity (time dependent effects) are widely discussed. Section 3 presents the mentioned three models of disordered magnetism, their assumptions, results and conclusions characteristic for them. Applications of the theories are included in Section 4 where some magnetic properties of selected magnetically soft and hard materials are shown and discussed.

2. Magnetism in low-dimensional systems

During last few years one can notice a strong development of low-dimensional physics that concerns thin layers, micro/nano structures on surface and in volume [4-7]. The common feature of the systems is a significant, in a comparison with bulk materials, contribution of surface. It is worth to plot the percentage contribution of surface as a function of average size of the object (counted in atoms and with the assumption that the lattice constant is 2 Å) which is depicted in Fig. 1.

One can see that the contribution of surface becomes significant for objects with diameter less than 10 nm. As a consequence of such effect one can indicate a change of electronic structure as well as an appearance of significant contribution of shape and surface magnetic anisotropy [8]. From magnetic point of view, it is important that the listed factors influence atomic interactions and what follows can affect magnetization and magnetic structures.

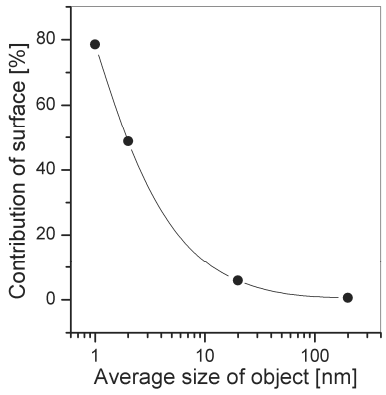

Fig. 1. Percentage contribution of surface as a function of average size of the object (with the assumption that the lattice constant is 2 Å)

2.1. Superparamagnetism

The term superparamagnetism refers to systems of noninteracting magnetic clusters or nanoparticles [8]. Usually, inside such objects magnetic moments are coupled (e.g. ferromagnetically) and therefore, one can consider them as one overall magnetic moment μ_{cl}. The values of μ_{cl} depend on atomic magnetic moments, magnetic structure within nanoparticle (or cluster) and its size. As examples of materials that reveal superparamagnetic properties one can indicate magnetic nanocomposites, diluted magnetics, natural rocks with magnetic impurities and some biological specimens (hemoglobin, ferritin…). Magnetization processes of superparamagnetic materials can be well described by the so-called Langevin function according to the following relation:

$$M(T,H) = n_{cl} \cdot \mu_{cl} \cdot \left(\coth x - \frac{1}{x} \right) = n_{cl} \cdot \mu_{cl} \cdot L(x) \quad , \quad x = \frac{\mu_{cl} \mu_0 H}{k_B T} \tag{1}$$

where M is the magnetization, T is the temperature, H is the external magnetic field, n_{cl} is the number of clusters per volume unit, μ_0 is magnetic permeability of vacuum, k_B is the Boltrzman constant and L is the Langevin function.

The argument of L expresses a competition between magnetic energy $\mu_{cl}\mu_0 H$ and thermal energy $k_B T$. Due to the lack of intergrain interactions $M(T)$ dependence (and what follows susceptibility χ) fulfill the Curie low as classical paramagnetics but with high magnetic moment. In contrary to this magnetic isotherms reveal saturation, like for ferromagnetics. This behaviour can be explained in this way that a large cluster magnetic moment causes relatively high energy of interaction between the cluster and external field, so in a given temperature the Langevin function saturates in relatively low H. Fig. 2 presents a set of magnetic isotherms calculated with different values of μ_{cl} (at $T = 2$ and $T = 300$ K).

As shown, magnetic clusters that possess overall magnetic moment of 20 μ_B well saturates at $T = 2$ K but at $T = 300$ K behave like paramagnetics. Saturation of $M(T)$, at this temperature, requires higher μ_{cl} i.e. in the order of 10^3 μ_B.

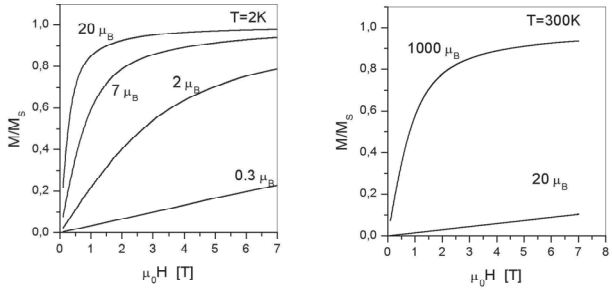

Fig. 2. Calculated magnetic isotherms (normalized to saturation M_S) for different values of μ_{cl} at $T = 2$ K and $T = 300$ K

More realistic case of superparamagnetic systems is the situation when clusters or nanoparticles possess magnetic anisotropy. This means that a change of direction of cluster magnetic moments requires some energy. In the simplest case of the uniaxial anisotropy the two stages e.g. parallel and antiparallel to H are separated by a kind of energy barrier E_B with a highest dependent of anisotropy coefficient K_U and cluster volume V ($E_B = K_U V$ see Fig. 3).

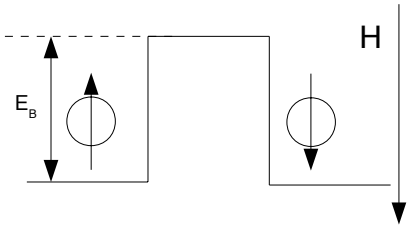

Fig. 3. A schematic picture of energetic barrier that separates parallel and antiparallel alignment of cluster magnetic moment

If the thermal energy $k_B T$ is comparable with the energy barrier E_B one can observe spontaneous jumps over the barrier. Dynamics of this process can be described by the simple relaxation formula:

$$\frac{dM}{dt} = -\frac{M}{\tau}, \quad \tau = \tau_0 \exp\left(\frac{E_B}{k_B T} \right) \tag{2}$$

where τ is the temperature dependent time constant.

Let assume that a typical measurement time t_p = 100 s. If $\tau < t_p$ than the system is superparamagnetic because thermal excitations allows rapid jumping over the barrier. Interesting is the case when $\tau > t_p$ and the jumps need some time or higher H. Generally, an apparent energy barrier depends also of the magnetic energy (forced by H) which will be discussed in the next paragraph. Nevertheless, in this condition the system is in the so-called blocking state. Taking a typical value of $\tau_0 = 10^{-9}$ s one can estimate the blocking temperature T_B below which magnetization depends on time:

$$T_B = \frac{V K_U}{25 k_B} \tag{3}$$

and the critical volume (at a given temperature) below which nanoparticles always are superparamagnetic (unblocked):

$$V_{kr}^{sp} \approx \frac{25\,k_B T}{K_U} \quad . \tag{4}$$

Table 1 presents the critical diameters $D_{kr}^{sp}=(6V_{kr}/\pi)^{1/3}$ for different magnetic materials [8].

Table 1.
Critical diameter of superparamagnetic nanoparticles for different materials

Material	D_{kr}^{sp} [nm]
α-Fe	16
Co	8
Ni	35
Fe_3O_4	4
$SmCo_5$	2

The blocking temperature, as an important parameter of superparamagnetic systems, can be determined from magnetization measurements in the ZFC-FC (the so-called zero field cooled and field cooled) procedure which is depicted in Fig. 4.

Starting from point #1 the sample is cooled down without H to point #2. In this point the field is switched on, the sample is heated and magnetization is recorded until temperature reaches point #3 (the ZFC curve). Next, the sample is again cooled down and magnetization is again measured. If the sample shows some blocking effects one can find a characteristic point in which the two curves (ZFC and FC) are separated. This point determines the blocking temperature T_B.

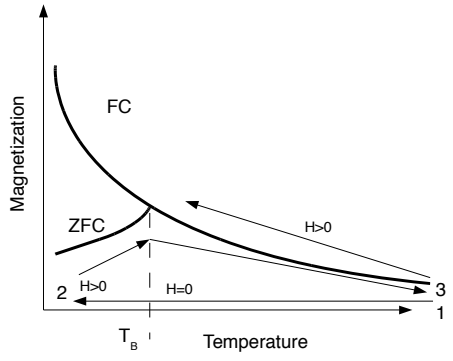

Fig. 4. Schematic diagram of ZFC-FC procedure (see the text)

In some cases (e.g. magnetic composites) a distribution of object size and what follows magnetic moments is expected. The total response of the material is a superposition of all kind of the objects with different magnetic moments:

$$M(H,T)=\sum_i N_i \cdot \mu_i \cdot L(x_i), \quad x_i = \frac{\mu_i \mu_0 H}{k_B T} \tag{5}$$

where N_i is the number (per volume unit) of objects with magnetic moment μ_i, H is the external magnetic field. Obviously, saturation magnetization $M_S=\Sigma_i N_i \mu_i$ plays the role of the normalization condition. The numbers N_i can be considered as a discreet distribution of magnetic objects in the analysed system. The other approach is to define a distribution function $\rho(\mu)$ (usually one can assume a Gaussian, log-normal or exponent function) and calculate magnetization by making use of the following equations:

$$M(H,T)=\int_0^\infty \rho(\mu)\cdot\mu\cdot L(x)\cdot d\mu, \quad x=\frac{\mu\mu_0 H}{k_B T} \tag{6}$$

with the normalization as $M_S=\int_0^\infty \rho(\mu)\cdot\mu\cdot d\mu$

Based on experimental $M(H)$ magnetic isotherms one can determine the numbers N_i or $\rho(\mu)$ function which is the main problem of the so-called Langevin granulometry [9]. From mathematical point of view it is an optimization problem i.e. how to find a proper magnetic moment distribution for which theoretical $M(H)$ curve fits to the empirical one. In this area there are several numerical methods that give physically reasonable results. One of very promising methods is the simulation annealing (SA) procedure with additional local entropy condition (for details see [10]). Summarizing the above one can state that the Langevin granulometry analysis allow determining not only distribiution of magnetic moments but also number of atoms (molecules) within the detected clusters. If crystal structure of the clusters is known it is possible to determine average size of the objects - this is the reason why such analysis is called granulometry.

2.2. The Stoner-Wohlfarth model of nanoparticles magnetization

The Stoner-Wohlfarth model [11] concerns magnetization processes of single domain particles in which a change of magnetization direction requires coherent rotation of atomic magnetic moments inside. Let assume that the shape of the particles is an ellipsoid with the main axis aligned along the z axis, as depicted in Fig. 5. Moreover, all further analysis are valid for $T = 0$ K.

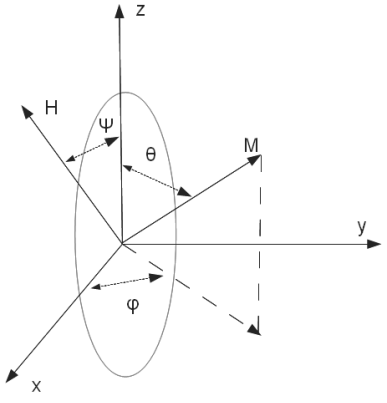

Fig. 5. Definition of directions and angles in the Stoner-Wolfarth model (see the text)

The key point in the model is to define proper energy terms in a function of θ (the angle between the applied magnetic field M and the ellipsoid axis z) and ψ (the angle between magnetization H and the ellipsoid axis z). Next, by a minimization of the energy (regards to θ) one can determine the direction of magnetization in a function of external magnetic field H, direction of H, and a shape of the particle. The important terms are magnetocrystalline anisotropy (let say uniaxial), shape anisotropy and magnetic energy:

$$\frac{E}{V} = K_1 \sin^2\theta - \frac{1}{2}\mu_0 M_S^2 N_{\parallel} \cos^2\theta - \frac{1}{2}\mu_0 M_S^2 N_{\perp} \sin^2\theta + \\ - \mu_0 M_S H\left(\cos\theta\cos\Psi + \sin\theta\sin\Psi\cos\varphi\right) \tag{7}$$

where K_1 is the uniaxial anisotropy coefficient, M_S is the saturation magnetization of the particle, $N_{\parallel}$ and $N\perp$ are the demagnetization factors parallel and perpendicular to the main axis, H is the external field. The first term in eq.(7) is related to magnetocrystalline anisotropy energy, the next two terms reflects the shape anisotropy of ellipsoid and the last one is the magnetic energy. Symmetry of the problem allows making a simplification (φ = 0) and consider the system as two dimensional in plane x-z. For these conditions one can get:

$$\frac{\partial E}{\partial \theta} = 2K_1 \sin\theta\cos\theta - \mu_0 M_S^2 \sin\theta\cos\theta(N_{\perp} - N_{\parallel}) + \\ - \mu_0 M_S H \sin(\Psi - \theta) \tag{8}$$

From the condition $\partial E/\partial\theta$=0 one can determine the so-called nucleation field H_N defined as a field necessary for changing direction of magnetization from parallel (to z axis) to antiparallel:

$$H_N = \frac{2K_1}{\mu_0 M_S} - M_S\left(N_{\perp} - N_{\parallel}\right). \tag{9}$$

Let analyse spherical particles as a specific case of ellipsoid where $N_{\parallel} = N\perp$. External field is applied in z direction. Fig. 6 shows calculated $E(\theta)$ dependences with different ratio of the magnetic energy $\mu_0 M_S H$ and the anisotropy coefficient K_1. When H = 0 energy of the system has the two equivalent minima at $\theta = 0$ and $\theta = \pi$. For $\mu_0 M_S H/K_1 = 1$ the system has one global energy minimum at θ = 0 but there is also a local minimum at $\theta = \pi$. Let notice that with increasing H the energy barrier between these two directions decreases and disappears for $\mu_0 M_S H/K_1$ =2. A position of the maximum of the energy barrier in a function of H is:

$$\theta_{max} = arccos\left(-\frac{\mu_0 M_S H}{2K_1}\right). \tag{10}$$

From the condition $\cos(\mu_0 M_S H/2K_1) \leq 1$ one can determine the so-called anisotropy field H_A for which the energy barrier disappears:

$$H_A = \frac{2K_1}{\mu_0 M_S}. \tag{11}$$

Important is also a value of the barrier $\Delta E = E_{max} - E(\theta=\pi)$ in a function if external field H which is:

$$\Delta E = K_1 V\left(1 - \frac{H}{H_A}\right)^2. \tag{12}$$

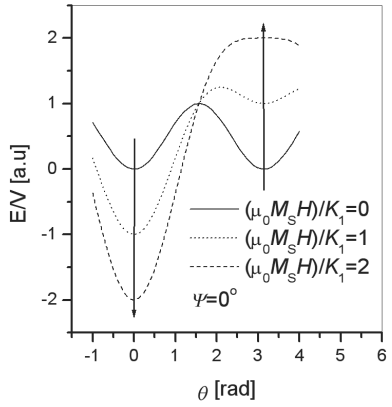

Fig. 6. $E(\theta)$ dependences with different ratio of magnetic energy $\mu_0 M_S H$ and anisotropy coefficient K_1 for ψ = 0, according to the Stoner-Wolfarth model

Magnetization of the particle is defined as a projection of M_S (aligned in the preferred by energy minimum angle θ) to the direction of H. Therefore magnetization curve $M(H)$ shows a rapid jump from $M = M_S$ to $M = -M_S$ at the anisotropy field.

Fig. 7 depicts magnetization curves for different values of the ψ - angle between external field H and the z axis which is also the easy magnetization axis. In real situations, samples consist of a set of nanoparticles with random distribution of their position and what follows easy magnetization axes. Total magnetization of such materials is a superposition of the curves presented in Fig. 7. Numerical simulations reveal that (at T = 0) for the system with randomly dispersed nanoparticles the remanence of magnetization (H = 0) $M_R = 0.5\ M_S$ and coercive field $H_C = 0.48\ H_A$ [12].

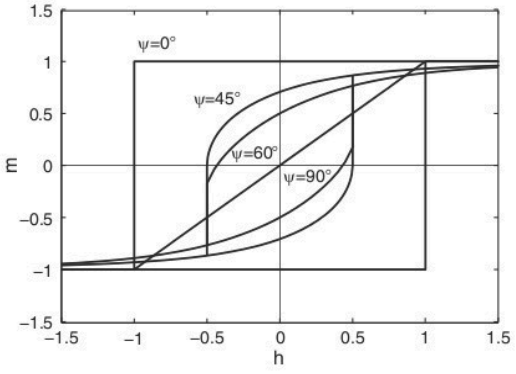

Fig. 7. Reduced magnetization $m = M/M_S$ vs. reduced field $h = H/H_A$ for different values of ψ calculated in the frame of the Stoner-Wolfarth model

2.3. Magnetic viscosity and time dependent effects

The fact that two directions of magnetization direction can be separated by an energy barrier ΔE is a source of the so-called time

dependent effects or magnetic viscosity [13-15]. According to the Stoner-Wolfarth model ΔE depends on magnetic anisotropy and energy of interaction between magnetization of the particle and external field H. The thermal energy (or thermal excitations) statistically can change magnetization direction with the probability proportional to $exp(-\Delta E/k_B T)$. So, the process can be activated by temperature or external field.

In the case of a single nanoparticle (or a set of identical particles) time dependent magnetization can be describe by formula (19) taking $E_B = \Delta E$. However, in real materials one can expect a contribution of different magnetic nanoparticles with different parameters which cause that the $M(t)$ response is a complex phenomenon with a continuous or discrete distribution of time constants. In the last case one can write:

$$M(t) = \sum_i M_{Si}\left[1 - \exp\left(\frac{-t}{\tau_i}\right)\right] \tag{13}$$

where $M(t)$ is related to an experiment where M increases, i counts kind of objects with the same time constant τ_i, M_{Si} is the magnetization of i-th component at $t = \infty$ (intensity of the relaxation) .

In some cases it is possible to obtain a proper analytical expression for $M(t)$. The necessary assumption are: i) uniform distribution of energy barrier $n(E) = n_E$ = const., ii) each objects contributes equally to the total magnetization and iii) magnetization measurements for $t > 0$ are performed without magnetic field. Accounting the above one can obtain:

$$M(t) - M(t_0) = m' n_E k_B T \ln(t - t_0) + const \tag{14}$$

where m' is saturation magnetization of the object. The quantity $n_E k_B T$ is called magnetic viscosity and can be determined as a slope of $M(\ln t)$ curve.

More precise analysis can be performed by making use of the so-called two-level model [16]. Let assume that material contain some magnetic objects that are characterized by total magnetic moment μ, activation energy (energy barrier) E_A and a number of such objects $N(\mu, E_A)$. Objects with the same μ and E_A can be analyzed as follows. Two magnetic states, let say X and Y, with different direction of magnetization are separated by the activation energy E_A and additional factor related to magnetic energy h of the particle (see Fig. 8). Not that the barrier is not symmetrical for the state X and Y. Dynamics of the system is described by kinetic equations:

$$\frac{dN_X}{dt} = W_{YX} N_Y - W_{XY} N_X$$
$$\frac{dN_Y}{dt} = W_{XY} N_X - W_{YX} N_Y \tag{15}$$

where N_X is the number of objects in state X, N_Y is the number of objects in state Y, W_{XY} is the frequency of jumps from X to Y, W_{YX} is the frequency of jumps from Y to X.

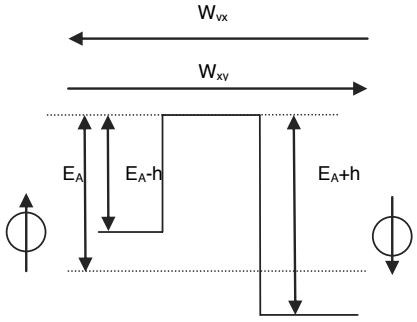

Fig. 8. Schematic diagram of the two-level model

The quantity W_{XY} and W_{YX} the canonical ensemble can be written as:

$$W_{XY} = W_0 \exp\left(-\frac{E_A - h}{k_B T}\right)$$
$$W_{YX} = W_0 \exp\left(-\frac{E_A + h}{k_B T}\right) \tag{16}$$

where h is the splitting of activation energy which may be caused by external magnetic field i.e. $h = \mu_0 \mu H$. Solution of the equations (15) is:

$$N_X = N\tau W_{YX} + (N_{X0} - N\tau W_{YX})\exp\left(-\frac{t}{\tau}\right) \quad , \quad \tau = \frac{1}{W_{XY} + W_{YX}} \tag{17}$$

where $N = N_X + N_Y$, $N_{X0} = N_X(t=0)$, τ is the time constant. Let consider the experiment where sample is magnetically saturated and next, magnetic field is switched to opposite direction at $t = 0$. State X is related to the objects that do not change their magnetic moments and state Y is related to the objects that change magnetic moments with the field. Magnetization is expressed by $M = \mu(N_Y - N_X)/V = \mu(N - 2N_X)/V$.

Now, we can introduce a distribution of both μ and E_A. Let divide ranges of the quantities into equally spaced channels with width $d\mu$ and dE_A, respectively. Let numbers of the channels are i for the μ space and j for the E_A space The distribution N_{ij} is a number of objects with magnetic moment $\mu = i \cdot d\mu$ and activation energy $E_0 = j \cdot dE_A$. The total magnetization is expressed as:

$$M = \sum_i \sum_j i\, d\mu \left(N_{ij} - 2N_X^{ij}\right) \tag{18}$$

where $N^{ij}{}_X$ is related to eq.(17) and eq.(16) in which $E_A \rightarrow j \cdot dE_A$ and $h = \mu_0 \mu H \rightarrow i \cdot d\mu\ \mu_0 H$.

It is worth to present a behavior of the system with a Gaussian distribution of μ and E_A:

$$N(\mu, E) = \frac{1}{2\pi\sigma_\mu \sigma_E} \exp\left[-\frac{(\mu - \mu_0)^2}{2\sigma_\mu^2}\right] \exp\left[-\frac{(E - E_0)^2}{2\sigma_E^2}\right]. \tag{19}$$

Fig. 9 depicts $M(t)$ curves calculated (using eq.(17)-(19)) with the distribution parameters: $\sigma_E = 0.1$ eV, $E_0 = 0.5$ eV, $\sigma_\mu = 300\ \mu_B$,

μ_0 = 2000 μ_B and W_0 = 10^9. This simulation concerns the experiment where sample is saturated to -M_S and next at t = 0 the field is switched off, so the $M(t)$ dependence is a relaxation of magnetization remanence.

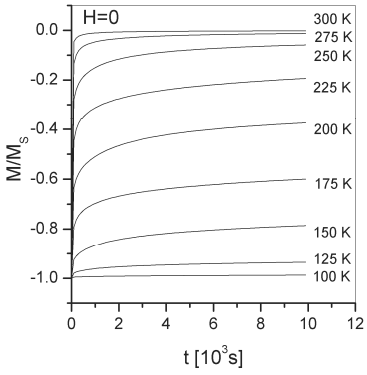

Fig. 9. Calculated M(t) curves in the frame of the two-level model (see the text)

As we can see at T = 100 K the thermal energy is to low (in a comparison with the activation energy) so magnetization remains unchanged after switching H. With the increase of temperature the thermal excitations activates some objects and the relaxation (non exponential) is observed. Intensity of the process, values of M_0=M(t=0) and M_R=M(t=∞) are related to a specific distribution $N(\mu,E_A)$, as shown in Fig.10. When H = 0 the magnetization relaxation do not depend on μ distribution and intensity of the process is a picture of energy cross of the distribution. Indeed, in our example the maximum occurs at $T \approx$ 200 K and the corresponding thermal energy ($25k_BT$) equals 0.45 eV which is close to the average value of $N(E_A)$ (E_0 = 0.5 eV).

Magnetic viscosity can also have an influence on thermomagnetic curves $M(T)$. Cooling or heating rate during measurements causes that the system is not in thermodynamic equilibrium. Therefore, the ZFC-FC procedure reveals some magnetic irreversibility that are connected with the rates of temperature changes and the $N(\mu,E_A)$ distribution. An example of such curves, calculated for the same case as in Fig. 14, for dT/dt = 2 K/min and $\mu_0 H$ = 1 T is presented in Fig. 11.

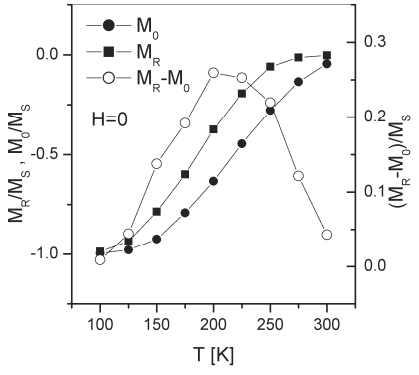

Fig. 10. Calculated intensity relaxation, values of M_0=M(t=0) and M_R=M(t=∞) in the frame of the two-level model (see the text)

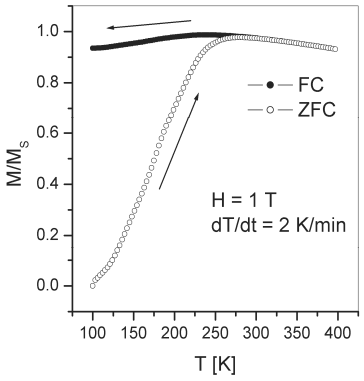

Fig. 11. Calculated ZFC-FC thermomagnetic curves in the frame of the two-level model (see the text)

3. Magnetism in disordered systems

Usually the term disorder is used in the context of the both structural (topological and/or chemical) and magnetic (interactions, anisotropy) properties failures. Typical materials influenced by the disorder are amorphous and nanocrystalline alloys, nanostructures of magnetic objects, nanoconposites, diluted magnetic materials and intermetallic compounds of rare earth and transition metals. Moreover, in polycrystalline samples some anomalies related to the area between the grains, which inherently carries some attributes of the disorder can be observed. Thus, knowledge of the subject presented here is essential for the proper analysis of magnetics with elements of disorder.

3.1. Random field Ising model

The random field Ising model (RFIM) is a development of the basic Ising model of ferromagnetism in which it is assumed that all spins in the system possess only two values of +1 or -1, let say up and down [17-19]. Furthermore, exchange interactions are included by the parameter J according to the Heisenberg model. Hamiltonian $\mathcal{H}$ of such system takes the form:

$$\mathcal{H} = -\sum_{j,i} J_{ij} S_i S_j - g\mu_0 \mu_B \sum_i H_i S_i \qquad (20)$$

where S_i, S_j are the spins at sites i and j, J_{ij} is the exchange parameter describing interaction between spins at sites i and j, H_i is magnetic field (internal or external) acting in site i., g is the Landé factor and μ_B is the Bohr magneton

The first term in eq. (20) expresses energy of interactions between spins. The summation over ij is usually spread out to the nearest neighbours due to short range nature of exchange coupling. The second term reflects magnetic energy. Disorder of the system can be introduced in the two places i.e. in distribution of exchange parameter J or external magnetic field H in the following way:

$$J_{ij} \propto J(|\boldsymbol{r_i} - \boldsymbol{r_j}|) \rightarrow J(|\boldsymbol{r_i} - \boldsymbol{r_j}|) + \delta J_{ij}$$
$$H_i \rightarrow H_i + h_i \tag{21}$$

where δJ_{ij} and h_i are random values of some distribution (usually with zero average), $\boldsymbol{r}_i$ and $\boldsymbol{r}_j$ are the position vectors. The case when the J parameter is disturbed will be discussed in next section as the random bond model. The RFIM model concerns the situation:

$$J_{ij} > 0 \quad , \quad \delta J_{ij} = 0 \quad , \quad h_i \neq 0 \tag{22}$$

Finally, without external magnetic field the Hamiltonian (20) is:

$$\mathcal{H} = -\sum_{j,i} J_{ij} S_i S_j - g\mu_0 \mu_B \sum_i h_i S_i \tag{23}$$

where these two terms describe a competition between ordering and introduced field disorder.

Probability of h_i is usually taken as Gaussian distribution:

$$P_G(h_i) = \frac{1}{\sigma_h \sqrt{2\pi}} \exp\left[\frac{-h_i^2}{2\sigma_h^2}\right] \tag{24}$$

or the so-called bimodal one:

$$P_{\mp}(h_i) = p\delta(h_i - h_0) + (1-p)\delta(h_i + h_1) \tag{25}$$

where δ is the Dirack delta symbol.

In the case $h_i >> J_{ij}S_j$ ferromagnetic ordering is impossible and spin system if frozen in random positions according to the randomness of h_i. Interesting is the case when the random field only slightly disturb ferromagnetic coupling. Let define the two important parameters i.e. correlation and autocorrelation spin function [20,21]. The first one expresses the average spontaneous magnetization $m = \langle\langle S_i \rangle_T\rangle_C$ where index T and C denotes averaging over temperature and configuration, respectively. The second parameter (called order parameter) $q = \langle\langle S_i \rangle_T^2\rangle_C$ reflects degree of freezing of the system. The value of parameter $q = 0$ indicates time changes of spin directions and $q = 1$ means that the spin position is the same at $t = 0$ and $t = \infty$. One can determine the different magnetic states in a function of the m and q parameters:

- for paramagnetic state $m = 0$ and $q = 0$,
- for ferromagnetic state $m > 0$ and $q > 0$,
- for "frozen" state $m = 0$ and $q > 0$

Introduced here the "frozen" state is the so-called spin-glass state in which the individual spins do not change direction (as in the ferromagnetic state), but spontaneous magnetization is zero (as in the paramagnetic state). The problems of spin-glasses are widely discussed in [22-32].

The starting point in calculations is to determine the free energy f as a function of the parameters m, q and disorder (as a distribution of fields h_i). From the condition of a minimum of f and with a given h_i distribution one can determine the equilibrium values of m and q. An analytical expression of f, calculated per one spin can be obtained with additional assumption that the summation in Hamiltonian (39) is spread over all $i \neq j$ (infinite range interactions), and $J_{ij} = J'/N$ (the requirement scaling due to the infinite range of interactions, N is a number of considered spins), so finally [33]:

$$f = J'm^2 - \frac{1}{\beta}\int dhP(h) \ln 2\cosh\left[\beta(2J'm + h)\right] \tag{26}$$

where:

$$m = \frac{1}{\beta}\int dhP(h) \tanh\left[\beta(2J'm + h)\right] \tag{27}$$

$$q = \frac{1}{\beta}\int dhP(h) \tanh^2\left[\beta(2J'm + h)\right] \tag{28}$$

and $\beta = 1/k_B T$.

Let analyze an influence of the field disorder, with the distribution defined by eq. (25), on magnetization process. Fig.12 shows a shape of free energy vs. m for an increasing contribution of the disorder. The parameters of the distribution are: $h = h_0 = h_1$, $k_B T = 1.4\ J'$, $p = 1/2$ and $J' = 1/2$. In the case without disorder ($h = 0$) and for a given temperature (related to J') the $f(m)$ function shows two equivalent energy minima close to ±1 which means that the considered system is almost saturated. At the same temperature and with increasing contribution of the random field (in relation to J') one can observe i) a decrease of the energy barrier separating the minima and ii) a simultaneously decrease of position of the minima. The later indicates decreasing of the average spontaneous magnetization. For $h = J'$ there is only one f-minimum at $m = 0$ which means that the field disorder causes fully random alignment of spins directions.

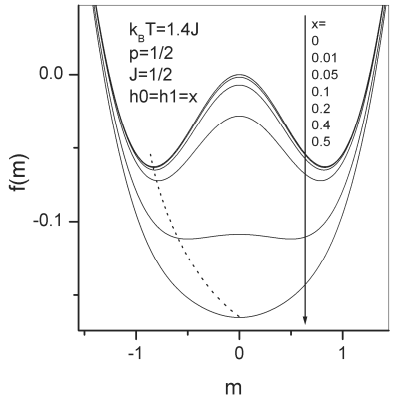

Fig. 12. Free energy vs. the parameter m calculated for different contribution of field disorder (see the text)

Fig. 13 presents calculated $m(T)$ curves for different values of h. One can observe a decrease of the Curie point with increasing contribution of the filed disorder. In the frame of the presented RFIM model one can also determine the order parameter q (Eq. (45)-(47)) as well as magnetic susceptibility χ by the following formula [33]:

$$\chi = \frac{\beta(1-q)}{1-2\beta J'(1-q)}. \tag{29}$$

Fig. 14 depicts some interesting temperature dependences of m, q and χ for different parameters of the random filed distribution (25).

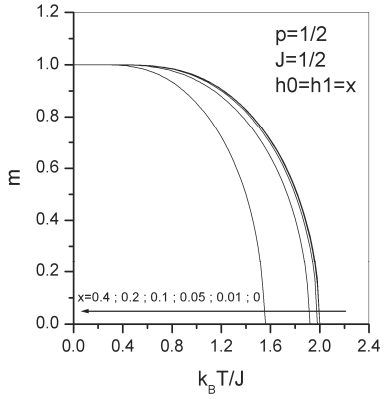

Fig. 13. Calculated $m(k_BT/J)$ for different values of h in the frame of RFIM model

In the case free of randomness i.e. $h = 0$ the m and q temperature dependences are typical for ferromagnetic materials (see Fig. 14a). Interesting is the situation with symmetric (p =0.5) field disorder ($h = 0.8\ J'$) when the q parameter has nonzero values while $m = 0$ (Fig. 14b).

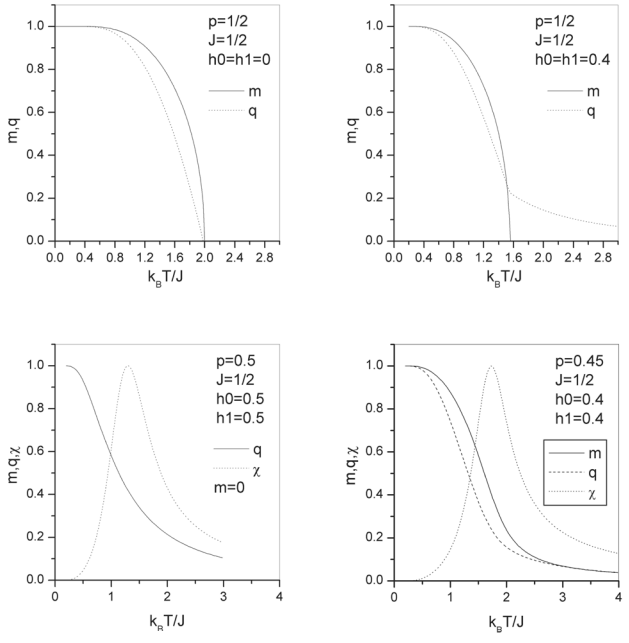

Fig. 14. Calculated temperature dependences of m, q and χ for different parameters of the random filed distribution (see the text)

It indicates frozen state in paramagnetic region. If $h = J'$ then $m = 0$ in the whole temperature range, however, magnetic susceptibility reveals a maximum that is related to freezing temperature (Fig. 14c). Let notice that, independently on exchange interactions, symmetric field disorder ($p = 0.5$) reflects a competition of up and down alignment of spins, so, can lead to a spin-glass-like magnetic structures. In contrary to this, antisymmetric filed disorder (e.g. $p = 0.45$) causes only a broadening of ferro-para transition, as shown in Fig. 14d.

3.2. Random bond model

The other approach consists in introducing a possible disorder as a distribution of the exchange parameter J_{ij} in Hamiltonian (23). Scott Kirkpatrick and David Sherington in the frame of the famous S-K model [34] have considered the following probability distribution:

$$P_G(J_{ij}) = \frac{1}{\sigma_J'\sqrt{2\pi}} \exp\left[\frac{(J_{ij}-J_0')^2}{2\sigma_J'^2}\right] \tag{30}$$

where J_0' is an average value (describing a contribution of ferromagnetism) and σ_J' is a standard deviation of the distribution. Similarly to the RFIM model the summation in (39) is spread over all $i \neq j$ (infinite range interactions) and therefore, the distribution parameters were normalized i.e. $\sigma' = \sigma_J/N^{1/2}$ and $J_0' = J_0/N$ (N is a number of spins). The starting point is to determine free energy of the system as a function of m, q and system disorder defined by (30). Generally free energy can be expressed as:

$$F = -k_b T\langle \ln Z\rangle = -k_B T\langle \ln tr \exp(-\beta \mathcal{H})\rangle \tag{31}$$

where Z is the statistic sum, the triangle brackets means configuration averaging. The statement $\langle \ln Z\rangle$ can be expressed as $\langle Z^n\rangle$ using the identity $\ln Z = \lim_{n\to 0}\left[\frac{1}{n}(Z^n - 1)\right]$. For integer n one can get $Z^n = \prod_{\alpha=1}^{n} Z_\alpha = tr_\alpha \exp(-\beta \sum_{\alpha=1}^{n} \mathcal{H}_\alpha)$ where α counts the so-called replicas of identical configuration (the "replica trick"). Now, the bond disorder is introduced as following:

$$\langle Z^n\rangle = tr_\alpha \prod_{i,j} dJ_{ij} P_G(J_{ij}) \exp\left(\beta J_{ij} \sum_\alpha S_i^\alpha S_j^\alpha\right). \tag{32}$$

After some manipulations one can obtain the following expression for free energy per site (spin):

$$f = k_B T[J_0 m^2/2k_B T - \sigma_J^2(1-q)/4(k_B T)^2 + \\ - (2\pi)^{-1/2}\int dz \exp(-z^2/2)\ln(2\cosh\eta)] \tag{33}$$

where $\eta = (J_0 m + \sigma_J q^{1/2} z + g\mu_0\mu_B H)/k_B T$, m and q satisfy the equations:

$$m = (2\pi)^{1/2} \int \mathrm{d}z \exp\left(-z^2/2\right) \tanh\eta \qquad (34)$$

$$q = (2\pi)^{1/2} \int \mathrm{d}z \exp\left(-z^2/2\right) \tanh^2\eta$$

Equations (34) can be solved using numerical methods. Fig. 15 shows an example for $J_0 = 0$ and $\sigma_J = 1$. Such distribution means the total disorder and the competition between ferromagnetic and antiferromagnetic interactions without preference of any of them. Clearly, the magnetization $m = 0$ in the full temperature range, while the order parameter q increases from zero (for $k_B T/\sigma_J = 1$) to unity (for $k_B T/\sigma_J = 0$). This is a typical paramagnetic - spin-glass transition ($m = 0$, $q > 0$), which is also confirmed by the susceptibility χ. It should also be emphasized that the presented model for the first time gave the compatibility of experimentals (including heat capacity) that confirms the random bond nature of disorder in the spin-glass systems.

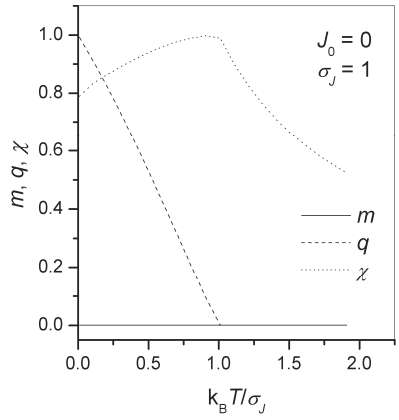

Fig. 15. Calculated temperature dependences of m, q and χ for symmetric distribution of exchange parameter (see the text)

Let analyze the system with antisymmetric distribution (30) i.e. $J_0 > 0$ which reflects a possible contribution of ferromagnetic interactions. Fig. 16 shows m, q and χ dependences for different ratio J_0/σ_J. For $J_0/\sigma_J = 1$ one can observe a typical paramagnetic - spin-glass transition at $k_B T = \sigma_J$. With the increasing contribution of ferromagnetism i.e. $1 < J_0/\sigma_J < 1.25$ there are two magnetic phase transition: para - ferro ($m > 0$, $q > 0$) at higher temperature and ferro - spin-glass ($m = 0$, $q > 0$) at lower temperature. For $J_0/\sigma_J > 1.25$ ferromagnetism of the system does not allow formation of the spin-glass structure. Such analysis leads to the phase diagram, shown in Fig. 17.

Despite the development of knowledge in the field of disordered magnetism the S-K model has some limitation where the solutions are instable (see [35], the A-T line). The reason lies in the "replica trick" or to say more precise the problem is in the identity of the system replicas. Therefore, there are some models that break the identity and give reasonable solutions in a broad range of temperature [36-39].

Other model (omitting the replica trick) was proposed by Thouless, Anderson and Palmer (TAP model [40]). The main difference lies in averaging of system disorder. In the S-K model the averaging is at the stage of calculation the statistical sum while the TAP method averages the disorder using the mean field procedure (MFA). In this approach one can write the set of equations:

$$\langle S_i \rangle_T = \tanh\left[\beta\left(\sum_j J_{ij} \langle S_j \rangle_T + g\mu_0 \mu_B H_i\right)\right] \qquad (35)$$

where the MFA means that $\langle f(S_j) \rangle_T \approx f(\langle S_j \rangle_T)$ (f is a function).

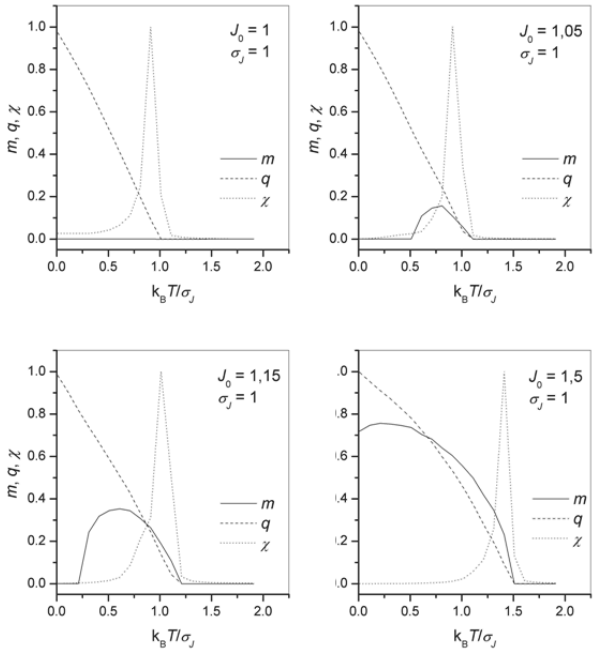

Fig. 16. Calculated temperature dependences of m, q and χ for different ratio J_0/σ_J (see the text)

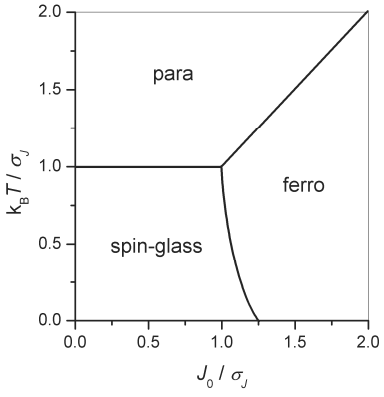

Fig. 17. Magnetic phase diagram calculated in the frame of the S-K random bond model

If $\langle S_i \rangle_T$ and J_{ij} do not depends on site eq. (35) express a typical thermomagnetic relation as for ordered ferromagnetics. In disordered systems the both conditions are not fulfilled.

Additionally, especially when $J_0 = 0$ it is necessary to take into account the so-called Onsager correction which describes reflexive interaction of the spin with the environment, so finally (for $H_i = 0$):

$$\langle S_i \rangle_T = \tanh\left[\beta\left(\sum_j J_{ij}\langle S_j\rangle_T - \beta\sum_j J_{ij}^2\left(1-\langle S_j\rangle_T^2\right)\langle S_i\rangle_T^2\right)\right]. \tag{36}$$

The ordering parameter q is defined as:

$$q = \frac{1}{N}\sum_i \langle S_i\rangle_T^2 . \tag{37}$$

Numerical analysis of equations (36) leads to some differences compared to the SK model. First of all, it is physically correct value of entropy that tends to zero at $T = 0$ and $\chi \to 0$ when $T \to 0$. Fig. 18 shows the differences in $\chi(T)$ curves calculated in the frames of the S-K and the TAP model [40].

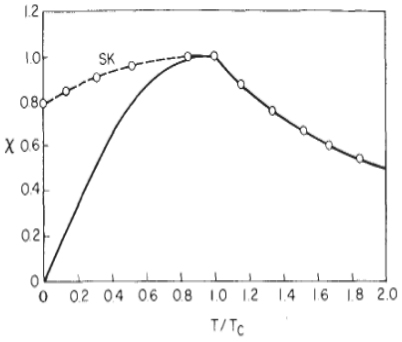

Fig. 18. $\chi(T)$ curves calculated in the frame of the S-K (dashed line) and the TAP model (solid line) [40]

3.3. Random anisotropy model (RAM)

Disorder in magnetic systems may also include magnetic anisotropy [41-44], especially important in the case of amorphous or nanocrystalline materials. In order to account this type of disorder it is necessary to write the Hamiltonian containing a term describing the anisotropy (for simplicity magnetocrystalline anisotropy):

$$\mathcal{H} = -\sum_{i,j} J_{ij}\boldsymbol{S}_i\cdot\boldsymbol{S}_j - \sum_i K_i(\boldsymbol{S}_i\cdot\boldsymbol{z}_i)^2 - g\mu_0\mu_b\sum_i \boldsymbol{H}_i\cdot\boldsymbol{S}_i \tag{38}$$

where K_i are local anisotropy constants $\boldsymbol{z}_i$ are unit vectors of easy magnetization axis on i site.

The anisotropy disorder can be introduced as a distribution of anisotropy coefficients or directions of easy magnetization axes. Surely, the later is more realistic, and therefore, this case will be discussed below in details.

In two dimensional case one can determine free energy of the system f with the assumption that $K_i = K$, $J_{ij} = J_{ex}$ and $\boldsymbol{z}_i$ are distributed randomly [45] and the result is:

$$f = -k_B T \max_{(r)}\left[\frac{-r^2}{2} + \int_0^{2\pi} d\,\frac{\theta}{2\pi}\ln g(r,\theta)\right] \tag{39}$$

where $g(r,\theta) = \int_0^{2\pi}\frac{d\varphi}{2\pi}\exp\left[\left(\frac{J_{ex}}{k_B T}\right)^{1/2} r\cos(\varphi-\theta) + \frac{K}{k_B T}\cos^2\varphi\right]$.

Equation (39) leads to the following expression of the m parameter:

$$m = \int_0^{2\pi}\frac{d\theta}{2\pi}\cos\theta\tanh\left(\frac{J_{ex} m}{k_B T}\cos\theta\right). \tag{40}$$

It is a characteristic feature that the random anisotropy do not change a temperature of para - ferro transition but only modify a shape of $m(T)$ dependence.

The effect of randomly distributed anisotropy axes lies in averaging out the anisotropy energy. Let denote the range of spatial correlations of spins as d, and magnetic correlations as L. For $L >> d$ in the range of the magnetic correlations there are different randomly oriented easy magnetization directions. On one hand, the anisotropy energy minimization requires spin alignment with the easy directions. On the other hand, this setting increases the energy of exchange interaction. The competition between the energies is responsible for the effectiveness of anisotropy averaging. Qualitatively, this can be expressed as follows. Anisotropy energy density is averaged in a cube with edge L to the value:

$$\langle E_A\rangle \sim K\left(\frac{d}{L}\right)^{3/2}. \tag{41}$$

Exchange energy density is:

$$\langle E_{ex}\rangle \sim \frac{A}{L^2} \tag{42}$$

where A is the sum of J_{ex}. Regarding (41) and (42) the minimum of energy occurs for:

$$L = \frac{16A^2}{9K^2 d^3}, \tag{43}$$

and consequently, inserting (43) to (41) one can get:

$$\langle E_A\rangle \sim \frac{K^4 d^6}{A^3}. \tag{44}$$

It should be stressed that the relation (44) is correct only if $L >> d$, i.e. for small K with respect to A (or J_{ex}). It may be noted that in some cases the disorder of local anisotropy can lead to a reduction in average anisotropy energy when exchange interactions are dominant. Otherwise, the magnetic correlation range will not include a sufficiently large number of spins and the equation (41) is not valid.

Three-dimensional problem of the Hamiltonian (38) can be successfully solved using computer simulation, which is the second approach of the analysis of systems with random

anisotropy axis. Using an algorithm such as the Monte Carlo (MC) one can obtain plots of magnetization as a function of applied field and temperature [46]. It turns out that parameters of magnetic hysteresis loops (coercive field H_c and magnetization remamence M_R) strongly depends on the ratio of the anisotropy constant K and the exchange parameter J_{ex}. As shown in Fig. 19, for $K/J_{ex} \approx 2$ there is a sharp jump of H_c, and for $K/J_{ex} > 10$, this parameter reaches a constant value independent on the anisotropy. At the same time the increasing of the ratio K/J_{ex} causes a decrease of magnetization remanence (Fig. 19) that reaches a plato of $M_R/M_S \approx 0.5$.

Averaging of anisotropy effect is also present in nanocrystalline materials. Similarly to the previous considerations, the randomness of the distribution of anisotropy axis direction concerns single grain, while the range of magnetic correlation includes a large number of such nanograins. In the frame of the well-known Herzer model [47-50] anisotropy is averaged (according to the random walk model):

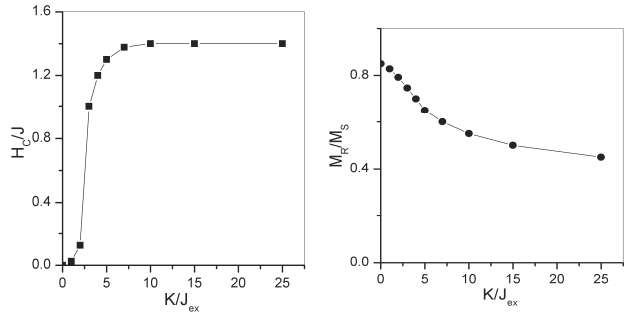

Fig. 19. Calculated dependence of coercive field and normalized remanence M_R/M_S on K/J_{ex} ratio

$$\langle K \rangle = \frac{K_{loc}}{\sqrt{N}} \tag{45}$$

where K_{loc} is a local anisotropy coefficient of single particle, N is a number of particles within the range of magnetic correlations L_{ex}. When D is a diameter of the particles $N=(L_{ex}/D)^3$. One can also determine the length of magnetic correlations:

$$L_{ex} = \varphi \sqrt{\frac{A}{\langle K \rangle}} = \varphi^4 \frac{A^2}{K_{loc}^2 D^3} = L_0 \left(\frac{L_0}{D} \right)^3 \quad , \quad L_0 = \varphi \sqrt{\frac{A}{K_{loc}}} \tag{46}$$

where φ is a constant reflecting symmetry of the effective anisotropy constant (<K>) ($\varphi = 1$ in the Herzer model, $\varphi = (4/3)^{1/2}$ in the Alben model). For alloys based on cobalt L_{ex} = 5-10 nm, and for iron-based alloys L_{ex} = 20-40 nm. Thus, both the amorphous materials (D is atomic scale) and nanocrystalline materials with nanoparticles (several nanometers) can fulfill the requirement of anisotropy averaging i.e. $L_{ex} > D$. Finally, including (46) in (45) the average anisotropy coefficient takes the form:

$$\langle K \rangle = \frac{1}{\varphi^6} \frac{K_{loc}^4 D^6}{A^3} = K_{loc} \left(\frac{D}{L_0} \right)^6 . \tag{47}$$

Let notice that the effective anisotropy is reduced with decreasing D ($\langle K \rangle \sim D^6$). Fig. 20 shows the dependence $\langle K \rangle(D)$ for FeSi (bcc) nanograins [49]. In this case, when D < 10 nm, the effective anisotropy is averaged to almost zero which results in significant improvement of soft magnetic properties.
The parameters that define the soft magnetic properties are coercivity and low-field magnetic permeability, both related to the anisotropy according to the following relations [49]:

$$H_C = p_C \frac{\langle K \rangle}{M_S} \approx p_C \frac{K_{loc}^4}{M_S A^3} D^6 \tag{48}$$

$$\mu_i = p_\mu \frac{M_S^2}{\langle K \rangle} \approx p_\mu \frac{M_S^2 A^3}{K_{loc}^4} \frac{1}{D^6} \tag{49}$$

where p_C and p_μ are dimensionless constants with the values close to unity.

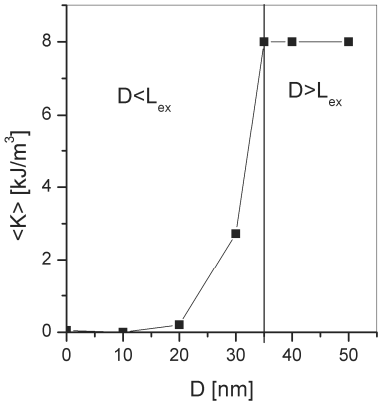

Fig. 20. Dependence $\langle K \rangle(D)$ for FeSi (bcc) nanograins

4. Examples of magnetic materials with structural and magnetic disorder

The development of modern technologies and the permanent tendency to reduce costs requires the use of soft magnets with parameters much better than the known conventional materials. Improvement of soft magnetic properties is possible in the case of amorphous and nanocrystalline materials, so for materials with significant contribution of disorder. Generally, a suitable nanostructure (chemical grain composition, their size and distribution, type of matrix) can lead, according to the Herzer model, to a significant reduction of magnetocrystalline anisotropy energy which causes a decrease of coercivity and increase of magnetic permeability (eq.(48),(49)). Enhancement of the parameters by a proper nanostructure is known as the optimization effect and occurs for many iron-based alloys that are the most promising magnetic materials (not only soft) and still are intensively studied. The optimization of soft magnetic properties can cause a reduction of energy losses in transformers, weight of electric motors, increase the efficiency of shielding of electromagnetic, magnetic and electric fields etc.

The other, important for application, magnetic materials are permanent magnets showing hard magnetic properties. Generally, hard magnets are used in power generators, electric motors, different kinds of sensors and data storage media. Such materials should be characterized by high coercivity, high value of saturation magnetization and remanence. The idea is that, after sample saturation, magnetic moments should be "trapped" after switching off the field. Therefore, any kind of magnetic anisotropy, as the energy barrier that causes the blocking of magnetic moments, is favorable to magnetic hardening. Also, in the group of hard magnetic materials a suitable nanostructure can significantly improve the characteristics required for the mentioned applications. Nanocrystalline alloys containing grains of hard magnetic phases combine different types of magnetic anisotropy, i.e. the magnetocrystalline, shape and surface anisotropy related to the grains and their boundary regions. In addition, the grain boundaries are a source of internal stresses, so-called thin domain walls, blocking the movement of domain walls and magnetic disorder. All these factors are advantageous for magnetic hardening.

In the next subsections selected magnetic materials with structural and magnetic disorder, their properties and analysis methods based on the Sections 2 and 3 are presented. The materials are divided into the four groups i.e. i) superparamgnetisc and diluted magnetic materials, ii) iron-based amorphous and nanocrystalline alloys as soft magnets, iii) iron based bulk nanocrystalline alloys as hard magnets and iv) magnetic nanocoposite.

4.1. Superparamagnetics and diluted magnetic materials

A good example of application of the Langevin granulometry method concerning superparamagetic systems (see Section 2.1) is analysis of distribution of magnetic moments in thin layers SiC/Mn deposited on Si substrate [10]. Let compare the two samples with 15.5% Mn content (denoted as Mn(Si)-1) and 26.8% Mn content (denoted as Mn(Si)-2). Fig. 21 shows original magnetic isotherms measured at T = 300 K. Thermomagnetic curves (not presented here) as well as the saturation character of the isotherms confirm superparamagnetic behaviour of the samples.

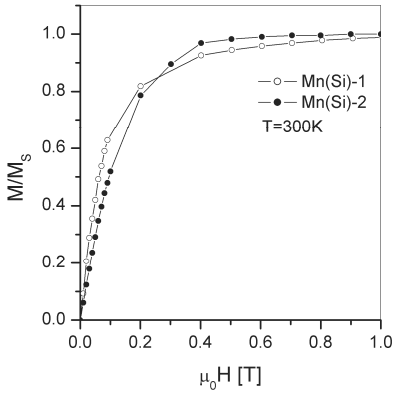

Fig. 21. Magnetic isotherms for thin layers Mn(Si)-1 (15.5 % Mn) and Mn(Si)-2 (28.6% Mn)

Results of the SA procedure are shown in Fig. 22. For the sample Mn(Si)-1 the distribution consists of the two Gaussian like components positioned at 2300 μ_B and 14000 μ_B. Assuming that magnetic moment of Mn atom is about 2.3 μ_B one can state that the clusters contain about 1000 and 6000 Mn atoms, respectively. For the sample Mn(Si)-2 the distribution reveals the one narrow peak at 7400 μ_B. On average, these clusters contain 3200 Mn atoms.

Langevin granulometry methods can be used not only for imaging of magnetic clusters, but also the system of noninteracting magnetic moments. An example can be the analysis of the distribution of magnetic moments in preparations of human blood. It is know that the blood contains iron mainly in the form of hemoglobin where the Fe ions are located in a central position of porphyrins. In [51] magnetic properties of blood of patients with and without atherosclerosis were carefully studied. Figs. 23 and 24 show an example of $M(T)$ and $M(H)$ curves at T = 2 K for the two representative samples.

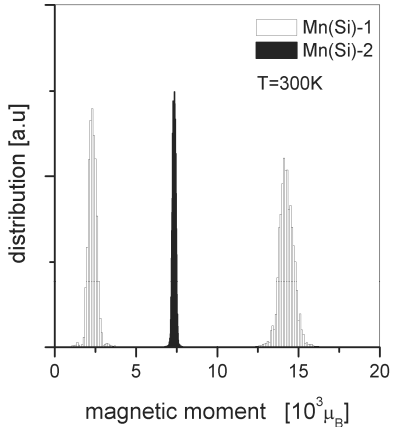

Fig. 22. Calculated distributions of magnetic moments obtained from the SA procedure (see the text)

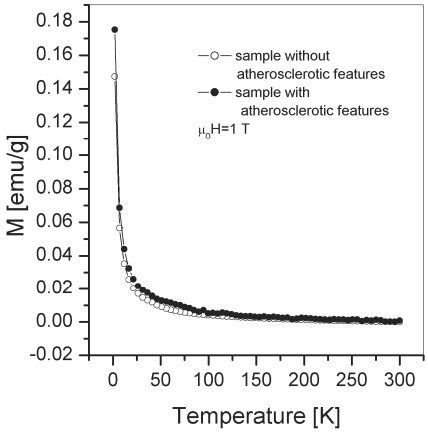

Fig. 23. Magnetization versus temperature for samples with (closed circles) and without (open circles) atherosclerotic features

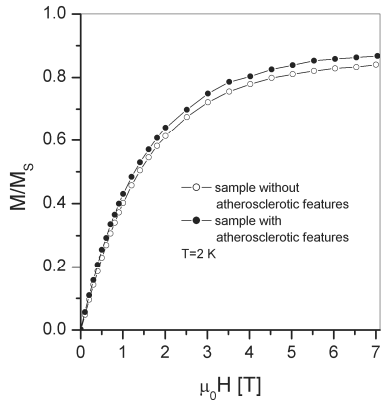

Fig. 24. Reduced magnetization M/Ms versus magnetic field for samples with (closed circles) and without (open circles) atherosclerotic features

As in the previous example, paramagnetic nature of the $M(T)$ curves allows applying the SA procedure in order to determine a distribution of magnetic moments (see eq.(5)). The results of such analysis are presented in Figs. 25 and 26. In the case of the "healthy" sample one can see the three Gaussian-like components located below 0.5 μ_B (related to a nonsaturated component of $M(H)$ curve), about 4 μ_B (related to hemoglobin) and approximately 7 μ_B (related to complexes of hemoglobin). For the sample of a person suffered from atherosclerosis the first two components are also present but the third one is not dedected. In addition, the position of the peak of hemoglobin is shifted into higher values, and its width is slightly higher. It is obvious that on the basis of several biological samples more general conclusions are impossible, however, the analysis show the usefulness of the algorithm to characterize the magnetic properties of such preparations.

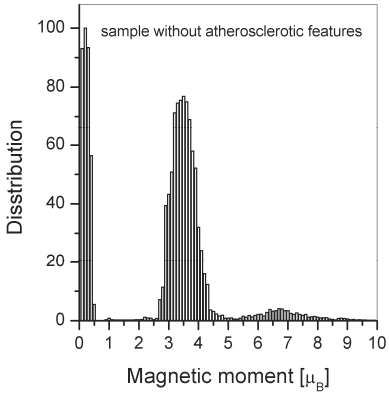

Fig. 25. Distribution of cluster magnetic moment for sample without atherosclerotic features

A third, quite an interesting example concerns aluminum-based diluted magnetic materials i.e. $Al_{87}Y_5Ni_8$, $Al_{87}Y_4Gd_1Ni_8$, $Al_{87}Gd_5Ni_8$, $Al_{87}Y_4Dy_1Ni_8$, and $Al_{87}Dy_5Ni_8$ amorphous alloys [52,53]. Figs. 27 and 28 show thermomagnetic curves $M(T)$ and inverse susceptibility $1/\chi$ for the mentioned above alloys, respectively. The $1/\chi$ temperature dependences reveal a deviation of the Curie-Weiss law in the low temperature range. However, in higher temperatures this law is well fulfilled and one can determine the so-called θ temperature (as a crossing point of the fitted $1/\chi$ line and the T-axis (see Fig. 28), that describes interactions. The origin of the interactions depends on a kind of material.

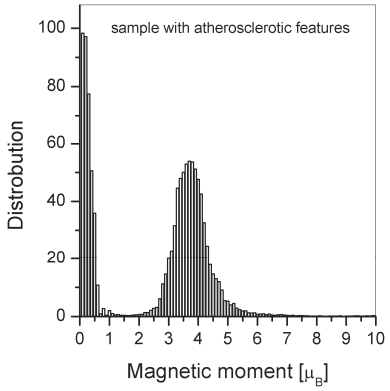

Fig. 26. Distribution of cluster magnetic moment for sample with atherosclerotic features

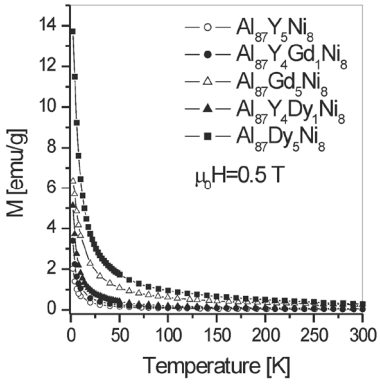

Fig. 27. Thermomagnetic curves $M(T)$ for selected aluminum-based amorphous alloys

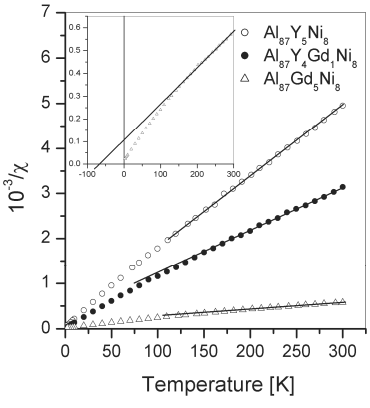

Fig. 28. $1/\chi$ vs. temperature for the selected aluminum-based amorphous alloys; in the inset: $1/\chi$ vs. T for the $Al_{87}Gd_5Ni_8$

In the case of diluted magnets with metallic matrix indirect RKKY and dipolar coupling are expected [30]. If the matrix is not conductive or for composites produced of magnetic powders only dipolar interactions can occur. Independently on the origin one can include the effect in analysis of superparamagnetic systems by replacing T with $T+\theta$ in the argument of the Langevin function (see eq.(1)). Fig. 29 depicts the magnetic isotherms from which determination of the distribution of magnetic moments were performed. The results of applying the SA Langevin granulometry procedure are shown in Fig. 30, where an influence of Dy alloying addition is presented. Note that the $Al_{87}Y_5Ni_8$ reference alloy contains two types of Ni clusters with average values of 10 μ_B and 88 μ_B. Because for this alloy, magnetic moment attributed to Ni is 0.3 μ_B (determined from the saturation magnetization [90]) the clusters contain about 35 and 300 Ni atoms. The addition of 1 at.% of Dy causes a shift of the both components in the lower values. This is due to the fact that Dy partially disturbs ferromagnetic coupling of Ni within the clusters, forcing antiferromagnetic arrangements of Dy-Ni magnetic moments. Therefore, the fragmentation of the Ni clusters is more effective for increasing Dy content which is particularly evident in the case of $Al_{87}Dy_5Ni_8$ alloy.

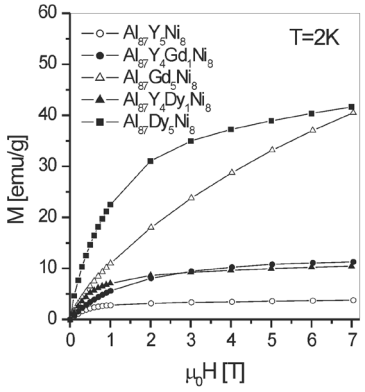

Fig. 29. Magnetic isotherms $M(H)$ for selected aluminum-based amorphous alloys, measured at 2 K

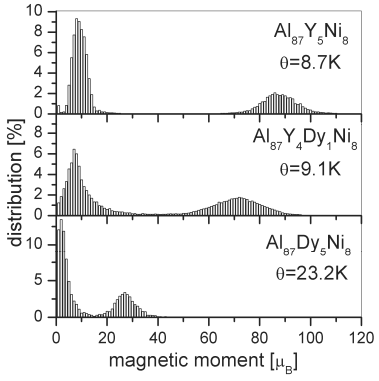

Fig. 30. Distribution of cluster magnetic moments for $Al_{87}Y_5Ni_8$, $Al_{87}Y_4Dy_1Ni_8$, and $Al_{87}Dy_5Ni_8$ alloys at 2 K

The presented examples do not exhaust the range of applications of Langevin granulometry, however, they show remarkable usefulness of this method in the characterization of magnetic systems. It should be noted that one of the major advantages of the analysis presented here is the possibility of indirect observations of magnetic objects that consist of even several atoms which for other direct methods can be difficult or impossible.

4.2. Amorphous and nanocrystalline alloys - soft magnets

Amorphous and nanocrystalline alloys containing magnetic elements are a very good example of materials for which properties are connected with the disorder either at the atomic level, or microstructure. These materials are usually prepared by melt-spinning technique in the form of thin amorphous strips and next, the nanostructure is obtained by isothermal (usually for one hour) annealing at temperatures close to the crystallization temperature. Very high initial relative permeability (up to 10^5), low coercivity (less than 10 A/m) and high saturation induction value (up to 2 T) place this type of alloys in the group of modern soft magnetic materials [54-63].

It is known that by appropriate alloying additions and annealing procedures one can affect their magnetic properties. It is a simple consequence of the fact that amorphous alloys are not in thermodynamic equilibrium and the annealing leads to changes of its microstructure. The material reaches thermodynamic equilibrium in two, broadly defined processes i.e. i) structural relaxation of the microstructure that occurs at temperatures up to the beginning of the crystallization and ii) crystallization. In some cases the microstructural changes occurring during annealing leads to the optimization effect [54-56, 59], which consists in simultaneous correlation of various material parameters - magnetic, electrical and mechanical in order to fulfil requirements of different applications.

Historically, the first nanocrystalline alloys, for which ferromagnetism was discovered were the FINEMET type containing Fe as the main element and Si, B,P… as additions [1, 55-59]. They are characterized by high initial magnetic permeability (about 10^4) and high saturation induction (about 1 T). In order to increase the saturation induction, in the so-called NANOPERM alloys type, the Si alloying addition is eliminated [1, 69-71]. Subsequently, in order to increase the Curie temperature, iron is partially replaced by cobalt which gives the new type of nanocrystalline alloys called HITPERM [1, 72-75]. Fig. 31 shows a comparison of soft magnetic properties for different type of materials [76]. Table 2 summarizes different magnetic and related properties of selected nanocrystalline alloys [77].

Generally, nanocrystalline materials show a brittleness resulting from high contribution of nanograins surface that obviously narrows the field of their applications down. However, it is possible to optimize the soft magnetic properties in the so-called relaxed amorphous phase without formation of nanostructures. This phenomenon was observed for the first time in NANOPERM type alloys [78]. A proper Nb content allows obtaining a relatively stable (thermodynamically) relaxed amorphous structure, which can combine some attributes of disordered structures (without a long range correlation) and ordered structures (reduction of internal stresses and excess volume - microvoids). In this structure there are interesting phenomena related to magnetism in systems with disordered magnetic anisotropy and exchange interactions (fluctuation of interatomic distances).

Table 2.
Crystallization temperature T_{x1} - the first stage, T_{x2} - the second stage, Saturation induction B_s, initial magnetic permeability μ, coercivity H_c, magnetostriction λ_s, crystallites diameter d and annealing temperature T_a for selected nanocrystalline alloys

Amorphous precursor	T_{x1}	T_{x2}	B_s	μ	H_c	λ_s	d	T_a
	[K]	[K]	[T]	10^{-3}	[A/m]	10^6	[nm]	[K]
$Fe_{92}Zr_8$	804	900	1.62	2	66		23	823
$Fe_{90}Zr_7B_3$	825	1025	1.63	22	5.6	1.1	18	933
$Fe_{85}Zr_7B_8$	861	993		19				673
$FE_{86}Zr_5B_8Cu_1$	750	870	1.54			0.5	13	823
$Fe_{86}Zr_7B_6Cu_1$	800	995	1.52	48	3.2	1	10	873
$Fe_{88}Zr_7B_3Al_2$	805	1020	1.57	11		0		873
$Fe_{86}Zr_7B_3Si_4$	815	1040	1.54	10		0.5		873
$Fe_{87}Zr_7B_2Si_4$	810	1050	1.56	14		0		873
$Fe_{89}Zr_7B_2Al_2$	800	1030	1.61	17		0		873
$Fe_{88}Zr_7B_2Si_2Al$			1.55	12		-1		873
$Fe_{87}Zr_7B_3Si_2Al$			1.52	11		-0.5		873
$Fe_{87}Zr_4Nb_3B_6$	802		1.50	3.5			15.9	923
$Fe_{86}Zr_4Nb_3B_6Cu_1$	757		1.54	18	3.7			923
$Fe_{86}Zr_{3.25}Nb_{3.25}B_{6.5}Cu_1$			1.61	110	2.0	-0.3	9	
$Fe_{85.6}Zr_{3.3}Nb_{3.3}B_{6.8}Cu_1$			1.57	160	1.2	-0.3	8	
$Fe_{84}Zr_{3.5}Nb_{3.5}B_8Cu_1$			1.53	120	1.7	0.3	8	
$Fe_{84}Nb_7B_9$	800	1070	1.4	9.8	220	0.4	8	923
$Fe_{84}Nb_7B_8Cu_1$	705	1045	1.48	16	8.9			823
$Fe_{83}Nb_7B_9Ga_1$			1.48	38	4.8		10	
$Fe_{83}Nb_7B_9Ge_1$			1.47	29	5.6	0.2	24	
$Fe_{83}Nb_7B_9Cu_1$			1.52	49	3.8	1.1	8	
$Fe_{84}Nb_{3.5}Zr_{3.5}B_8Cu_1$			1.53	100	1.7	0.3	19	
$Fe_{85}Nb_{3.5}Hf_{3.5}B_7Cu_1$			1.44	92	1.3	0.2	20	
$Fe_{90}Hf_7B_3$			1.59	32	4.5	-1.2	13	
$Fe_{56}Co_7Ni_7Zr_{10}B_{20}$	890		0.96	18	2.4			750
$Fe_{60}Co_3Ni_7Zr_{10}B_{20}$	870				5			
$Fe_{49}Co_{14}Ni_7Zr_{10}B_{20}$	895				11			
$Fe_{46}Co_{17}Ni_7Zr_{10}B_{20}$	905				12			

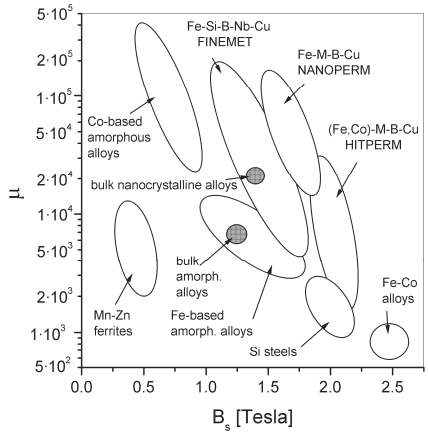

Fig. 31. Comparison of the soft magnetic properties of amorphous and nanocrystalline materials (according to [76])

Optimization effect - the relaxed amorphous phase

A typical example is the $Fe_{86-x}Nb_x\ B_{14}$ ($2 \leq x\ 8$) group of NANOPERM type alloys. The samples of $Fe_{86-x}Nb_x\ B_{14}$ ($2 \leq x\ 8$) (NANOPERM type) were prepared by melt-spinning technique as amorphous ribbons with thickness and width of about 20 μm and 1 cm, respectively The amorphicity of the as quenched alloys was confirmed by XRD as well as Mössbauer spectroscopy measurements [79-81]. Soft magnetic properties and a potential for optimization of these properties were examined by the experiment consisting of i) preliminary isothermal annealing for one hour at T_a ranging from 300 K to 900 K (the so-called 1-hour annealing temperature) and ii) measurements of magnetic permeability and other properties at the room temperature. Fig. 32 shows the obtained optimization curves for $Fe_{86-x}Nb_x\ B_{14}$ ($x = 2, 6, 8$). The term optimization refers to initial magnetic permeability μ (determined at room temperature) and reflects the observed significant increase of μ in a function of T_a. Notice, the highest value of μ was obtained for the $Fe_{80}Nb_6B_{14}$ alloy preliminary annealed at $T_a = T_{op} = 700$ K/1h (T_{op} is the optimization temperature). In a comparison with the as quenched state (assumed $T_a = 300$ K) in the optimized state (or optimized microstructure) μ increases about 13 times reaching the value of $33 \cdot 10^3$.

Such optimization effect in literature is usually attributed to a formation of nanostructure of α-Fe nanograins embedded into amorphous ferromagnetic matrix. In our case the effect occurs just in amorphous phase which was proofed by applying different

experimental techniques. For example, the performed electron microscopy observations (image and diffraction pattern of HRTEM) reveal that for $Fe_{80}Nb_6B_{14}$ alloys annealed at $T_a = T_{op} = 700$ K the microstructure is fully amorphous (see Fig. 33). The first nanograins were observed for $T_a = 760$ K, so 60 K above T_{op}. For $T_a = 840$ K a well formed nanostructure of α-Fe was detected.

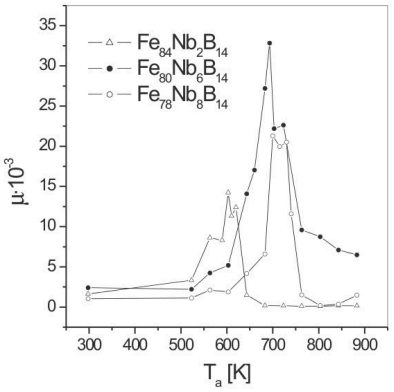

Fig. 32. Optimization curves for $Fe_{86-x}Nb_x B_{14}$ (x = 2, 6, 8) amorphous alloys

Thermomagnetic curves of amorphous and nanostructured magnets are a source of important information. Due to the structural disorder one can expect relatively low the Curie temperature (see Section 3.1), so in the case of iron-base amorphous alloys, the crystallization process is observed as an increase of magnetization with increasing T.

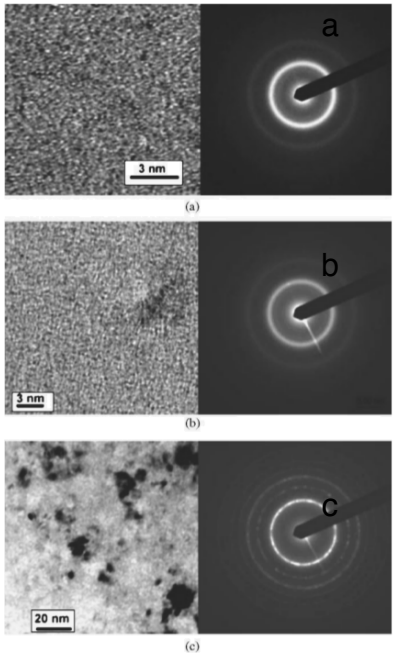

Fig. 33. Electron microscopy observations (image and diffraction pattern of HRTEM) for $Fe_{80}Nb_6B_{14}$ annealed at $T_a = 700$ K (a), $T_a = 760$ K (b) and $T_a = 840$ K (c)

Fig. 34 presets such $M(T)$ curves for $Fe_{80}Nb_6B_{14}$ preliminary annealed at different T_a. As shown, the depicted dependences reveal both T_C of amorphous phase and the crystallization temperature T_x (the first stage). Moreover, for the sample in the as quenched state the paramagnetic region between T_C and T_x confirms the absence of any Fe nanograins (for Fe $T_C = 1042$ K), so amorphicity of the alloys. The nonzero magnetization between T_C and T_x reveals a contribution of nanograins (which was observed for T_a >770 K/1h. This fact also confirms the optimization of soft magnetic properties in amorphous phase. Similar results were obtained for other examined here alloys.

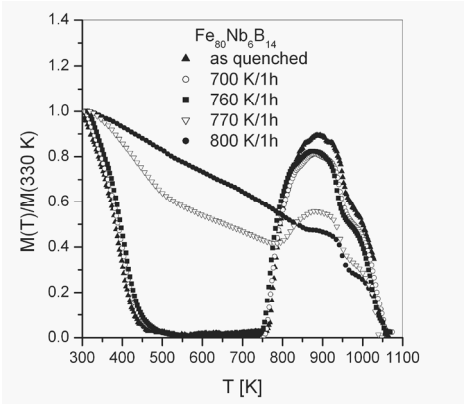

Fig. 34. $M(T)$ curves for $Fe_{80}Nb_6B_{14}$ amorphous alloy preliminary annealed at different T_a

It is worth to plot some magnetic quantities (measured at room temperature) as a function of T_a. Fig. 35 depicts such analysis of T_C, saturation induction $\mu_0 M$, time instabilities of μ, coercivity H_C and μ. The time instabilities of μ were determine as $\Delta\mu/\mu = (\mu(t_2)-\mu(t_1))/\mu(t_1)$ where $t_1 = 30$ s and $t_2 = 1800$ s after demagnetization. This quantity is related to internal stresses and free volume concentration. One can divide the structural changes into three temperature regions. The first one up to a significant decrease of $\Delta\mu/\mu$ (700 K) due to the structural relaxation (reduction of internal stresses and free volume), the second one up to the increase of T_C connected with the relaxed amorphous phase (RAP) (700 K - 760 K), and the third region attributed to the nanocrystallization (above 760 K). From the presented dependences it is evident that the optimization temperature T_{op} is placed in the RAP range. The relatively stable RAP results from the fact that Nb that slows down of diffusion processes, and therefore, the crystallization does not overlap the relaxed amorphous stage. Different properties connected with the RAP phase are discussed in [82-87].

A possible origin of the optimization effect that occurs in RAP can by studied based on the ZFC-FC magnetization measurements (see Section 2.1) [86]. As it was shown the ZFC-FC effect can be caused by magnetic disorder as well as anisotropy of nanosized magnetic objects (section 3.3). The original ZFC-FC curves for $Fe_{80}Nb_6B_{14}$ amorphous alloy are shown in Fig. 36. The difference of the two curves appears just at T_C which suggests some contribution of magnetic irreversibility effects without well defined blocking temperature. However, the difference defined as $(M_{FC}-M_{ZFC})/M_{ZFC}$ and measured for samples annealed at different T_a reveal some characteristics (see Fig. 37). As we can see, there are the two characteristic temperature regions: above and below 50 K.

Let analyze the sample annealed at T_a = 770 K for which the $M(T)$ dependence reveals some contribution of ferromagnetic Fe nanograins (see Fig. 34). In the T range 50-400 K the ZFC-FC effect almost does not occur but in lower temperatures a sharp increase is observed. It can be connected with the already formed nanograns and boundary regions between the nanograins and amorphous matrix (magnetic anisotropy disorder and/or frustrations of particles magnetic moments). It is characteristic that with the progress of structural relaxation (i.e. increase of T_a) one can observe a successive disappearing of the ZFC-FC effect that can be attributed to a reduction of internal stresses and free volume content. In contrary to this, the component at $T < 50$ K remains independent on T_a. It seems that the component is caused by small Fe clusters (for $T_a < 770$ K) and next at higher T_a the clusters serve as nucleation centers of the nanograins growing. Taking into account the above, one can conclude that in the case of Fe-Nb-B type of amorphous alloys the reduction of internal stresses and the formation of Fe clusters, that plays the same role in the Herzer model (described in Section 3.3) as nanostructure, cause averaging out of magnetic anisotropy that directly leads to optimization effect in relaxed amorphous phase.

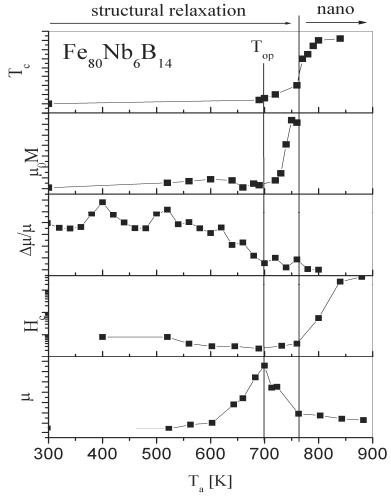

Fig. 35. Different magnetic quantities (measured at room temperature) as a function of T_a (see the text)

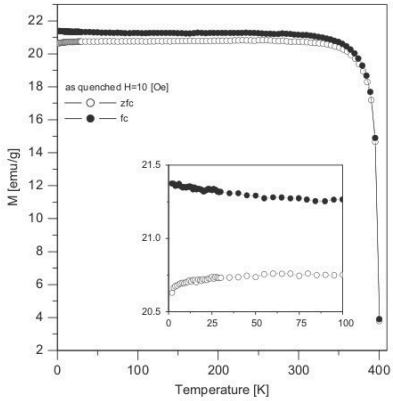

Fig. 36. ZFC-FC curves for $Fe_{80}Nb_6B_{14}$ amorphous alloy

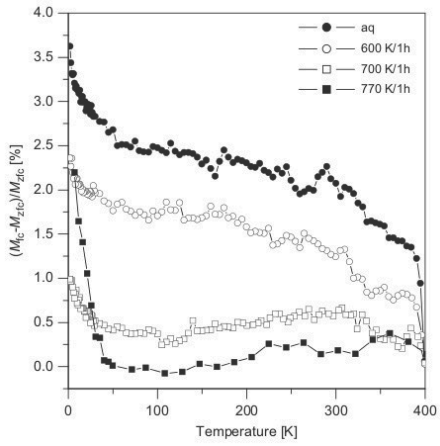

Fig. 37. $(M_{FC}-M_{ZFC})/M_{ZFC}$ curves and measured for $Fe_{80}Nb_6B_{14}$ amorphous alloy annealed at different T_a

Optimization effect in nanostructure

According to the Herzer model, soft magnetic properties can be enhanced by a specific nanostructure. In the case when the formed nanograins are oriented at random and ferromagnetic correlation length is spread over some number of grains, magnetocrystalline anisotropy is averaged according to Eq. (47). The condition $L_{ex} > D$ shows that favorable to magnetic softening are nanograins with diameter in order of 10 nm and ferromagnetic matrix (extention of L_{ex}). Fig. 38 shows pictures of microstructure for $Fe_{73.5}Cu_1Nb_3Si_{13.5}B_9$ (a), $Fe_{73.5}Cu_1NbSi_{16.5}B_6$ (b) (annealed at T_a = 810 K), $Fe_{74.5}Nb_3Si1_{3.5}B_9$ (c) (T_a = 800 K) and $Fe_{73.5}Cu_1Nb_3Si_{13.5}B_9$ (c) (T_a = 1170 K) [49]. From the selection only (a) and (b) fulfill the condition of averaging out of anisotropy and therefore, for these alloys the optimization effect occurs.

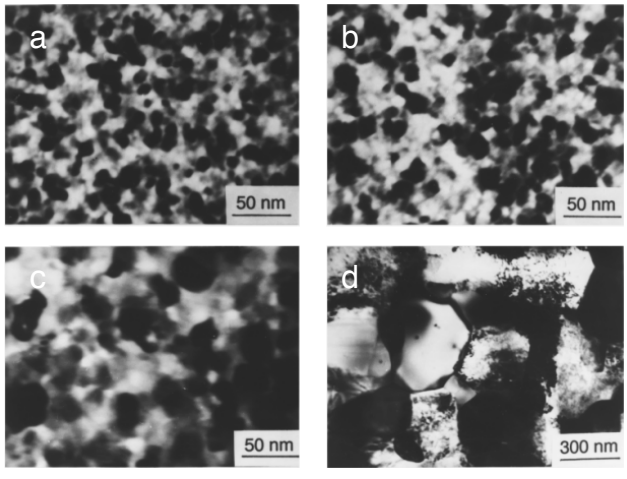

Fig. 38. Electron microscopy images for selected FINEMET type of alloys (see the text) [49]

A good examples of the materials for which the optimization effect is attributed to the nanostructure are the $Fe_{74}Cu_1Zr_3Si_{13}B_9$

FINEMET type alloy and $Fe_{76}Zr_2B_{22}$ NANOPERM type alloy [88]. The optimization curves for these alloys are presented in Fig. 39. The both alloys show the maximum of μ in the vicinity of nanostructure that is documented in Fig. 40. The HRTEM images revels the formation of nanograins of Fe-Si for $Fe_{74}Cu_1Zr_3Si_{13}B_9$ and Fe for $Fe_{76}Zr_2B_{22}$. In the both cases the mean diameters of the particles are about 3 nm.

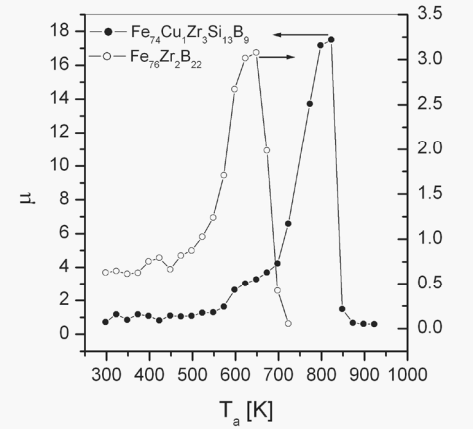

Fig. 39. Optimization curves for $Fe_{74}Cu_1Zr_3Si_{13}B_9$ and $Fe_{76}Zr_2B_{22}$ amorphous alloys

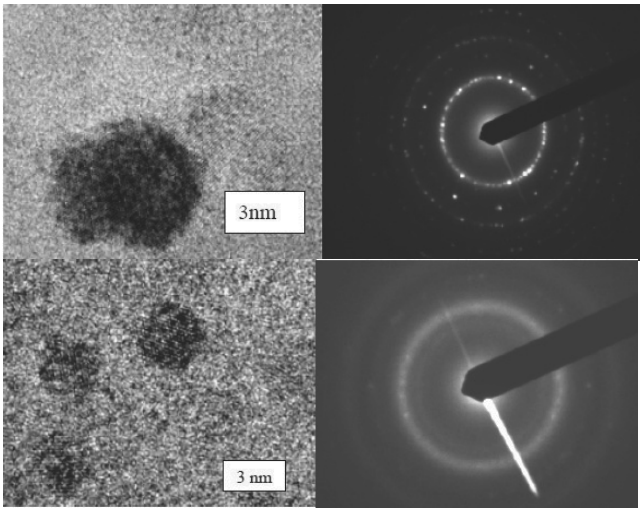

Fig. 40. HRTEM images for $Fe_{74}Cu_1Zr_3Si_{13}B_9$ (top) and $Fe_{76}Zr_2B_{22}$ (bottom) alloys, both in the optimized state

The random anisotropy (Herzer) model predicts also the dependences of coercivity and magnetic permeability on the grand dimension (eq.(48) and eq.(49)). These relations are in agreement with experimental results, which were tested for different nanocrystalline iron-based alloys, as depicted in Fig. 41. Let notice that for the grain size less that 50 nm the dependences follow as D^6 [48]. So, for the FINEMET type of alloys this value can be considered as a critical dimension below which the condition $L_{ex} > D$ is well fulfilled.

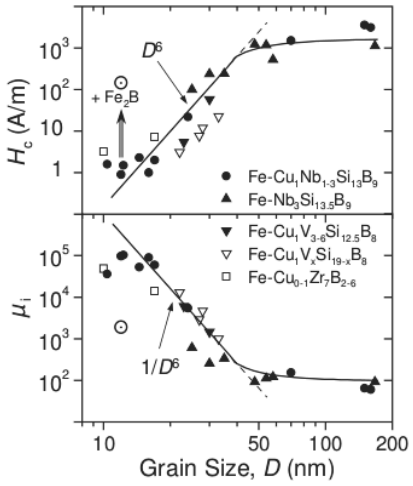

Fig. 41. Coercivity and initial magnetic permeability as a function of grain size diameter for different nanocrystalline alloys [48]

Influence of rare earth additions (R) on magnetic properties of Fe-Nb-B-R amorphous alloys

In order to study the influence of R elements on magnetic properties of the Fe-Nb-B type of amorphous alloys the samples of $Fe_{82}Nb_2B_{14}Y_2$ (as reference), $Fe_{82}Nb_2B_{14}Gd_2$, $Fe_{82}Nb_2B_{14}Tb_2$ and $Fe_{82}Nb_2B_{14}Dy_2$ were prepared by melt spinning technique [89]. Amorphicity of the alloys were tested and confirmed by XRD diffraction measurements. The aim was to test two kind of R additions i.e. without (Gd) and with (Tb, Dy, as heavy rare earths) so-called spin-orbit coupling [2]. In crystal structure Yttrium plays the same role as the other additions but is nonmagnetic. Therefore, the alloys with Y are the reference one showing similar microstructure without R-Fe magnetic interactions. Fig.42 presents magnetic isotherms for the examined alloys determined at T = 2 K. As shown, saturation magnetization decreases, in a comparison with Y sample, following the sequence: Gd, Dy and Tb. This effect is expected taking into account antiferromagnetic coupling of R-Fe.

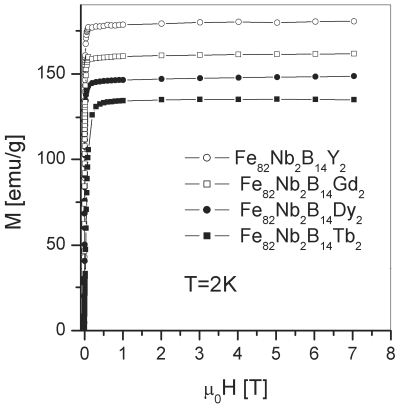

Fig. 42. Magnetic isotherms for the examined amorphous alloys determined at T = 2 K

The Curie temperatures and the crystallization temperature (heating rate 5K/min) of the alloys are about 450 K and 800 K, respectively (see Fig. 43). Moreover, these temperatures weakly depend on the alloying additions (2 at.%).

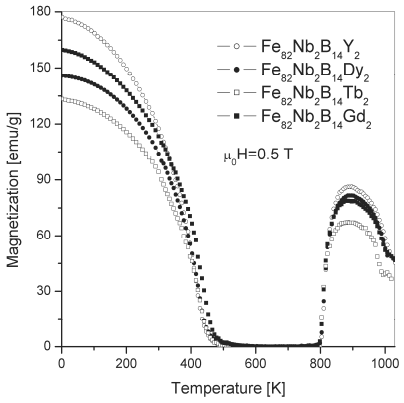

Fig. 43. Thermomagnetic M(T) curves for the examined amorphous alloys

In contrary to this, the presented in Fig. 44 relative ZFC-FC effect ($(M_{FC}$-$M_{ZFC})/M_{ZFC}$), determined in H = 10 Oe, is strongly influenced by the R additions. For Dy and Tb alloys one can observed a remarkable magnetic irreversibility i.e. at T = 2 K over 50%.

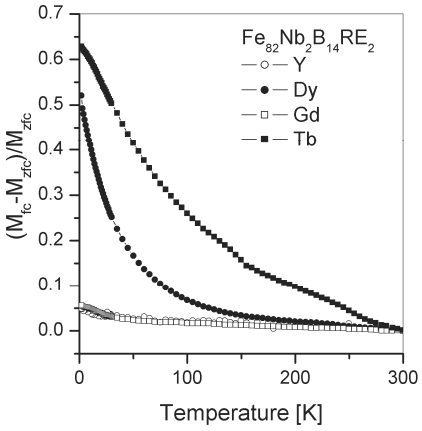

Fig. 44. Relative ZFC-FC effect, determined in H = 10 Oe, for the examined amorphous alloys

Table 3 summarizes the determined magnetic properties i.e. the Curie temperature T_C, saturation magnetization M_S, magnetic moment calculated per magnetic atom μ_m (Fe+R), magnetic moment calculated per Fe atom μ_{Fe} (assuming that the R additions safe their free ionic magnetic moment and antiferromagnetic coupling of R-Fe), magnetic permeability μ (determined from AC magnetic measurements; frequency about 1 kHz, magnetic field 0.5 A/m) and the relative change of the ZFC-FC curves at 2 K. Let notice that, except the $Fe_{82}Nb_2B_{14}Tb_2$ alloy, the magnetic moment calculated per Fe atom is almost constant and equals to about 2 μ_B,. The initial magnetic permeability is relatively low for the $Fe_{82}Nb_2B_{14}Tb_2$ and $Fe_{82}Nb_2B_{14}Dy_2$ alloys in a comparison with the $Fe_{82}Nb_2B_{14}Y_2$ and $Fe_{82}Nb_2B_{14}Gd_2$ alloys. One can divide the alloys into two groups i.e. alloys with Y, Gd and Tb, Dy. The difference between the groups is magnetocrystalline anisotropy introduced by the spin-orbit coupling (Tb, Dy) and structural disorder. It seems that the anisotropy energy is higher than exchange interactions energy and therefore the averaging of anisotropy (see eq.44) causes the observed deterioration of soft magnetic properties.

Table 3.
The determined magnetic properties of the alloys examined i.e the Curie temperature T_C, saturation magnetization M_S, magnetic moment calculated per magnetic atom μ_m (Fe+RE), magnetic moment calculated per Fe atom μ_{Fe}, magnetic permeability μ and the relative change of the ZFC-FC curves $(M_{FC}$-$M_{ZFC})/M_{ZFC}$ at 2 K

Alloy	T_C [K] ±1	M_S [emu/g] ±1	μ_m [μ_B] ±0.02	μ_{Fe} [μ_B] ±0.02	μ ±1	$(M_{FC}$-$M_{ZFC})/M_{ZFC}$ [%]
$Fe_{82}Nb_2B_{14}Y_2$	416	180	2.00	2.00	530	5.5
$Fe_{82}Nb_2B_{14}Gd_2$	450	161	1.79	2.04	750	4.9
$Fe_{82}Nb_2B_{14}Dy_2$	423	149	1.66	1.96	110	52.3
$Fe_{82}Nb_2B_{14}Tb_2$	430	135	1.51	1.77	160	62.7

The mentioned local magnetocrystalline anisotropy has an influence on magnetic domain structure. Fig. 45 shows representative pictures of the domains obtained from the Kerr microscopy observations. One can see that for the $Fe_{82}Nb_2B_{14}Y_2$ and $Fe_{82}Nb_2B_{14}Gd_2$ alloys the domain structure is quite "regular" and the magnetization tends to align parallel to the ribbon axis. In contrast to this for the samples with Tb and Dy the so called finger-print domains are observed. It is characteristic that the finger-print domains, decrease of μ and increase of ZFC-FC effect is connected with the anisotropy introduced Tb and Dy.

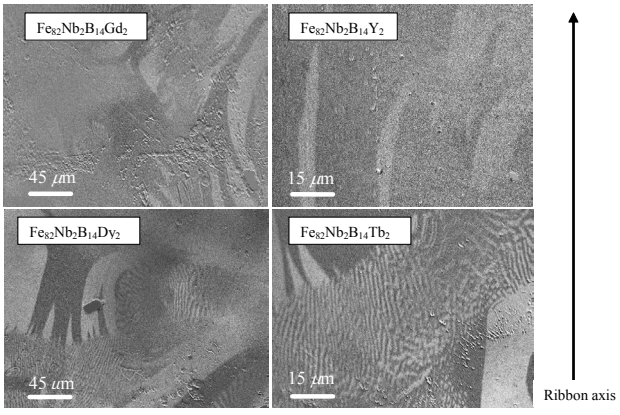

Fig. 45. Magnetic domain patterns obtained from the Kerr microscopy observations for the examined amorphous alloys

Summarizing the above one can state that the addition of 2 at.% of Tb or Dy leads to significant magnetic hardening of the examined alloys in amorphous phase.

However, in the alloys the optimization of soft magnetic properties effect occurs which is documented in Fig. 46. As we

can see Dy and especially Tb as alloying additions cause a decrease (in relation to the alloy with Y) of maximum μ about 2 and 4 times, respectively.

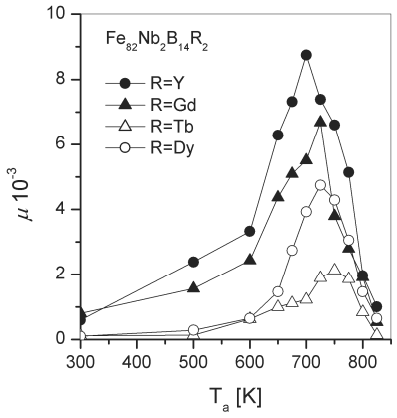

Fig. 46. Optimization curves for the examined amorphous alloys

Aging effect in nanostructure and relaxed amorphous phase

From application point of view interesting is an influence of aging on soft magnetic properties. In the studies reported in [90] two groups of alloys for which optimization effect occur in nanostructure ($Fe_{73.5}Cu_1Zr_{1.7}Si_{13}B_9$) and RAP ($Fe_{80}Nb_6B_{14}$) were tested. The examinations lie in determination of the optimization curves after aging (at room temperature) for several years (8 years for nanostructure and 3 years for RAP) and a comparison with these obtained just after casting. Fig. 47 shows such comparison for $Fe_{73.5}Cu_1Zr_{1.7}Si_{13}B_9$ amorphous melt spun ribbon aging for 8 years. One can see a stable optimization effect around the T_{op} and some instability in temperatures related to structural relaxation range (i.e. up to 800 K).

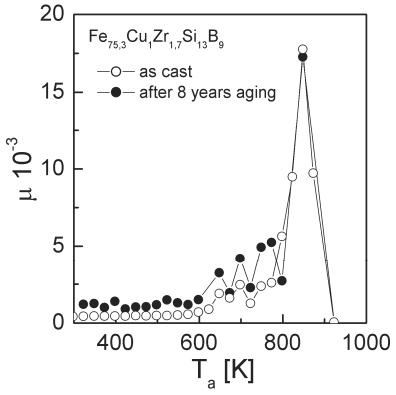

Fig. 47. Magnetic permeability m (H = 0.5 A/m) measured at room temperature for samples annealed for 1 h at temperature T_a for the $Fe_{73.5}Cu_1Zr_{1.7}Si_{13}B_9$ amorphous alloy

In contrary to this, for the $Fe_{80}Nb_6B_{14}$ alloy (aged for 3 years) significant changes in optimization curves were observed, as shown in Fig. 48. In fact, for samples annealed at T_a ranging from 500 K to 700 K magnetic permeability increases (after aging) even 2 times. It is also characteristic that the optimization effect is quite stable in temperatures corresponding to nanocrystallization (above 760 K).

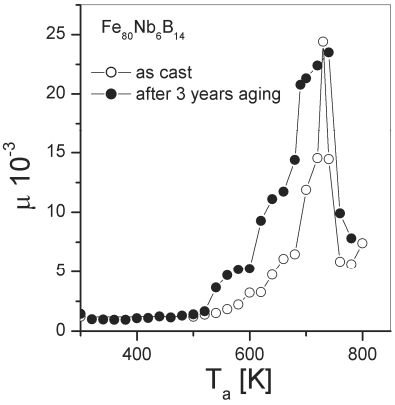

Fig. 48. Magnetic permeability m (H = 0.5 A/m) measured at room temperature for samples annealed for 1 h at temperature T_a for the $Fe_{80}Nb_6B_{14}$ amorphous alloy.

Because the optimization effect is connected with microstructure the presented results indicate thermodynamic phase stability of nanostructured magnets and some instability for structures related to degree of structural relaxation. This means that diffusion processes activated by the 1-h annealing occur even at room temperature but the crystal ordering requires much more time.

4.3. Bulk nanocrystalline alloys - hard magnets

The other applications of disordered materials are the field of permanent magnets. From this point of view any kinds of magnetic anisotropy is desirable. Obviously, materials that show high magneticrystalline anisotropy coefficient are magnetically hard, however, a proper nanostructure and sample technology can introduce additional anisotropy factors such as surface and shape anisotropy as well as a specific interaction between hard and soft phases (so-called spring-exchange [91,92]) that are favorable to further magnetic hardening. Many researches indicate that in this area very attractive are classical and nanostructured alloys and compounds based on transition and rare earth elements. Generally, the atoms of transition metals (Fe, Co) are the source of a large magnetic moment, while the rare earth metal atoms are the source of magnetocrystalline anisotropy [2]. Interesting are the two types of compounds of lower symmetry than the cubic system, i.e. $R_2Fe_{14}B$ with tetragonal structure and RCo_5 (or RCo_7) with hexagonal structure (R - rare earth element). However, not all rare earth elements in these compounds result in the strong anisotropy. It depends on the sign of the anisotropy constant K_1 i.e. when $K_1 < 0$ the magnetization vector lies in the plane perpendicular to the *c* axis of the crystal structure and there is no energy barrier that prevents changing the direction of

magnetization [2]. This means that only compounds for which the constant $K_1 > 0$ can be used as materials for permanent magnets. For the compounds of the $R_2Fe_{14}B$ type: $K_1 > 0$ for R = Ce, Pr, Nd, Tb, Dy, Ho and $K_1 < 0$ for R = Sm, Er, Tm, Yb. For the RCo_7 and RCo_5: $K_1 > 0$ for R = Sm, Er, Tm, Yb and $K_1 < 0$ for R = Ce, Pr, Nd, Tb, Dy, Ho.

Table 4 and Table 5 present magnetic properties of selected hard magnetic materials and $R_2Fe_{14}B$ compounds family, respectively [93].

Table 4.
Magnetic properties of selected hard magnetic materials (BH_{max} - maximum energy product, B_r - remanence induction and H_c - coercivity)

Material	BH_{max}	B_r	H_c
	kJ/m^3	mT	kA/m
31/2% Cr Steel	1.03	1030	56
3% Co Steel	3.02	970	13
17% Co Steel	5.49	1070	18
38% Co Steel	7.79	1040	191
Ceramic 2	14.30	290	224
Ceramic 6	19.50	320	57
Alnico4	10.70	560	318
PtCo	71.60	645	20
Vicalloy 1	6.36	750	20
Remalloy	7.95	970	42
Cunife1	11.10	550	202
MnAlC	39.80	545	358
$SmCo_5$	160	900	696
$Nd_2Fe_{14}B$	320	1300	1120

Table 5.
Magnetic properties of $R_2Fe_{14}B$ compounds family (P - dencity, B_s - saturation induction, μ - magnetic moment, H_a - anisotropy field and T_c - The Curie temperature)

Compound	ρ	B_s	μ	H_a	T_c
	g/cm^3	T	μ_B/f.u.	MA/m	K
Ce_2Fe_14B	7.81	1.16	22.7	3.7	424
$Pr_2Fe_{14}B$	7.47	1.43	29.3	10	564
$Nd_2Fe_{14}B$	7.55	1.57	32.1	12	585
$Sm_2Fe_{14}B$	7.73	1.33	26.7	-	612
$Gd_2Fe_{14}B$	7.85	0.86	17.3	6.1	661
$Tb_2Fe_{14}B$	7.93	0.64	12.7	28	639
$Dy_2Fe_{14}B$	8.02	0.65	12.8	25	602
$Ho_2Fe_{14}B$	8.05	0.86	17.0	20	576
$Er_2Fe_{14}B$	8.24	0.93	18.1	-	554
$Tm_2Fe_{14}B$	8.13	1.09	21.6	-	541
$Y_2Fe_{14}B$	6.98	1.28	25.3	3.1	565

Preparation and phase structure of Fe-Nb-B-R bulk alloys

One of the frequently used in practice preparation method of bulk nanocrystalline alloys is the vacuum suction casting [94]. Schematic diagram of such apparatus id depicted in Fig. 49. Sample in the form of a ball is placed in the cooper mould (1) with a hole of diameter ranged from 0.5 mm to several mm. Next, the sample is melted by electric arc in the chamber with an inert gas and than the applied vacuum sucks the sample into the hole. Finally, the obtained samples are in the form of rods usually with length about 3 cm. The proper cooling rate is ensured by permanent cooling the mould by water (2). The cooper net (3) allows flowing of the gas but it serve as a stopper for the melted sample. An example of the obtained sample is presented in Fig. 50.

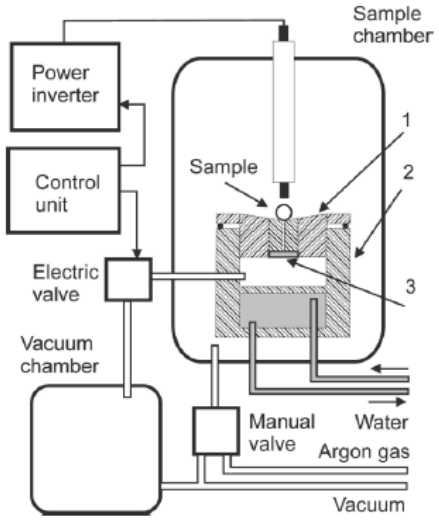

Fig. 49. Schematic diagram of the vacuum suction casting apparatus (see the text)

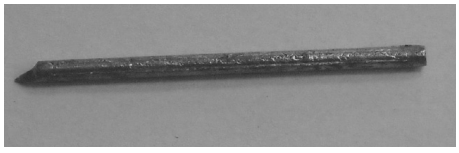

Fig. 50. An example of a sample obtained by the vacuum suction casting apparatus

Bulk nanocrystalline alloys of $(Fe_{80}Nb_6B_{14})_{1-x}M_x$ (M=Ni, Ag, Gd, Tb) are materials for which nanostructure leads to magnetic hardening [95,96]. Phases identification were performed with the use of XRD measurements, Mössbauer spectroscopy and high temperature $M(T)$ curves. From the thermomagnetic curves one can determine different magnetic phases with different T_C, as shown in Fig. 51. Interesting are the cases of Gd and Tb additions where the two magnetic phases with $T_C \approx 640$ K and $T_C \approx 810$ K for Gd and $T_C \approx 620$ K and $T_C \approx 730$ K for Tb. These temperatures are related to $R_2Fe_{14}B$ and RFe_2 phases.

More precise analysis of the XRD patterns as well as Mössbauer spectra reveal the formation of the ternary $R_2Fe_{14}B$, binary RFe_2, paramagnetic Fe and some intermediate phases. Table 6 summarized the detected phases and additionally, mean diameters of the formed crystallites (determined form broadening of XRD peaks) are also included. From magnetic point of view important are the alloy with Tb and the contribution of magnetically hard $Tb_2Fe_{14}B$ and the other relatively soft phases that are presented in Fig. 52. One can observe significant changes of the phases with the increase of Tb content i.e. decrease of $Tb_2Fe_{14}B$, increase of Tb_2Fe and almost constant amount of paramagnetic Fe.

Table 6.
Crystal phases, percentage contribution of a given phase (obtained from Mössbauer spectra or XRD patterns*) and mean diameter of the main phase *D* for the selected bulk alloys

Alloy	D [nm]	Phases	Contribution [%]
$(Fe_{80}Nb_6B_{14})_{0.92}Gd_{0.08}$	28	$Gd_2Fe_{14}B$, Int.Phase,$GdFe_2$ Para.	77, 6, 5, 12
$(Fe_{80}Nb_6B_{14})_{0.84}Gd_{0.16}$	13	$Gd_2Fe_{14}B$, Int.Phase,$GdFe_2$, Para.	59, 11, 17, 13
$(Fe_{80}Nb_6B_{14})_{0.68}Gd_{0.32}$	26	$GdFe_2$, Gd *	
$(Fe_{80}Nb_6B_{14})_{0.92}Tb_{0.08}$	28	$Tb_2Fe_{14}B$, $TbFe_2$, Para.	80, 8, 12
$(Fe_{80}Nb_6B_{14})_{0.84}Tb_{0.16}$	16	$Tb_2Fe_{14}B$, $TbFe_2$, Para.	59, 28, 13
$(Fe_{80}Nb_6B_{14})_{0.68}Tb_{0.32}$	25	$TbFe_2$, Tb_xFe_{2-x}, Para.	83, 7, 10
$(Fe_{80}Nb_6B_{14})_{0.92}Ni_{0.08}$	12	Fe-Ni (bcc), Fe-B, Para.	55, 34, 11
$(Fe_{80}Nb_6B_{14})_{0.84}Ni_{0.16}$	12	Fe-Ni (bcc/fcc), Fe-B, Para.	52, 36, 12
$(Fe_{80}Nb_6B_{14})_{0.68}Ni_{0.32}$	14	Fe-Ni (fcc), Fe-B, Para.	52, 42, 6
$(Fe_{80}Nb_6B_{14})_{0.92}Ag_{0.08}$	16	Fe (bcc), Fe-B, Paramag.	42, 49, 9

This tendency is a key point for controlling magnetic properties of the $(Fe_{80}Nb_6B_{14})_{1-x}Tb_x$ alloys. Moreover, the materials can be considered as nanocomposites with hard and soft magnetic phases for which some phenomena related to interactions between these phases are expected to be present.

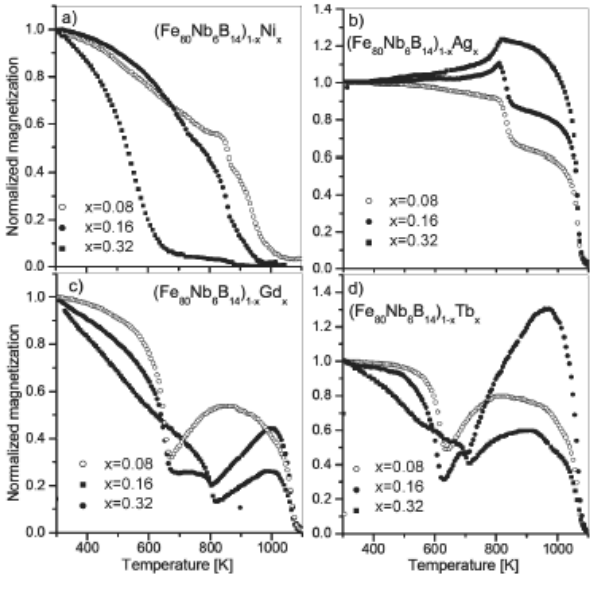

Fig. 51. High temperature $M(T)$ curves for $(Fe_{80}Nb_6B_{14})_{1-x}$ M_x (M=Ni, Ag, Gd, Tb) bulk alloys

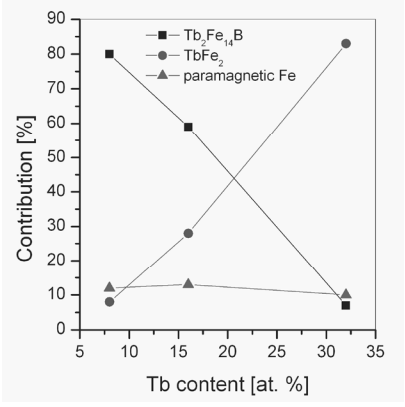

Fig. 52. Percentage contribution of the main phases for $(Fe_{80}Nb_6B_{14})_{1-x}Tb_x$ (x=0.08, 0.16, 0.32) bulk nanocrystalline alloys

Magnetic properties of Fe-Nb-B-Tb bulk nanocrystalline alloy

Magnetic properties of the $(Fe_{80}Nb_6B_{14})_{1-x}Tb_x$ ($0.02 \leq x \leq 0.32$) bulk nanocrystalline alloys will be discussed based on hysteresis loops measured at room temperature and at lower temperatures [97]. Figs. 53a-53d show the hysteresis loops for some selected alloys. One can see a variation of different magnetic parameters (coercivity H_C, saturation magnetization M_S, remanence magnetization M_R, $|BH|_{max}$) with the change of Tb content. These parameters depend on temperature which suggests a contribution of blocking effects described in Section 2.3.

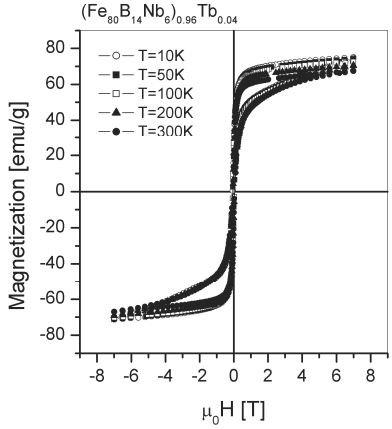

Fig. 53a. Hysteresis loops for $(Fe_{80}Nb_6B_{14})_{1-x}Tb_x$ (x = 0.04) bulk nanocrystalline alloys

Indeed, for $x > 0.08$ one can observe a significant increase of H_c with decreasing temperature. This means that in this case magnetization is a thermal activated process and in lower temperatures requires higher external field which results in the observed increase of H_C. Interesting are also shapes of the hysteresis loops that are different from those characteristic for classical ferromagnetic materials. As it was mentioned the alloys contains different magnetic phases i.e. magnetically hard $Tb_2Fe_{14}B$, and soft Tb_2Fe compound. Therefore, for some balance between

these phases the observed shapes of the hysteresis indicate superposition of the components with different magnetic properties. Obviously, the rapid jump of the $M(H)$ curve is attributed to the Tb_2Fe and other soft phases while H_c is related to the $Tb_2Fe_{14}B$.

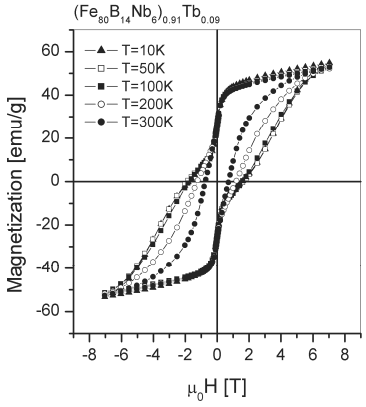

Fig. 53b. Hysteresis loops for $(Fe_{80}Nb_6B_{14})_{1-x}Tb_x$ (x = 0.09) bulk nanocrystalline alloys

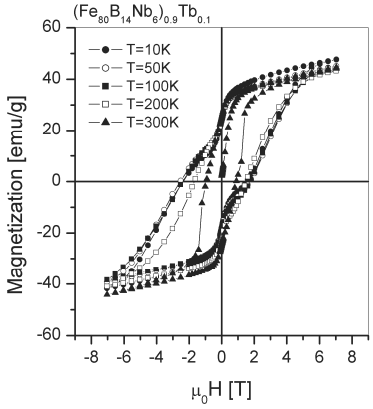

Fig. 53c. Hysteresis loops for $(Fe_{80}Nb_6B_{14})_{1-x}Tb_x$ (x = 0.1) bulk nanocrystalline alloys

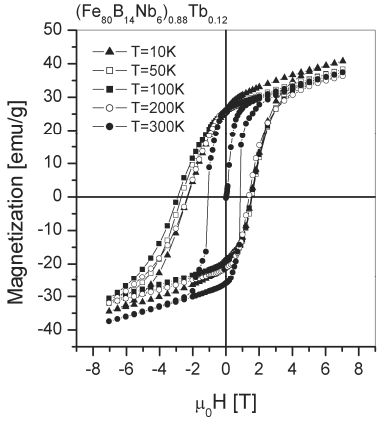

Fig. 53d. Hysteresis loops for $(Fe_{80}Nb_6B_{14})_{1-x}Tb_x$ (x = 0.12) bulk nanocrystalline alloys

Fig. 54 shows the of H_C and M_S determined at 300 K and 10 K versus Tb content, while normalized remanence magnetization M_R/M_S and $|BH|_{max}$ also versus Tb content are presented in Fig. 55.

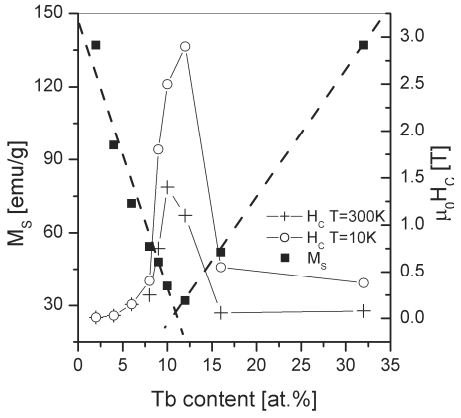

Fig. 54. M_S and H_C determined at 300 K and 10 K for $Fe_{80}Nb_6B_{14})_{1-x}Tb_x$ bulk nanocrystalline alloys

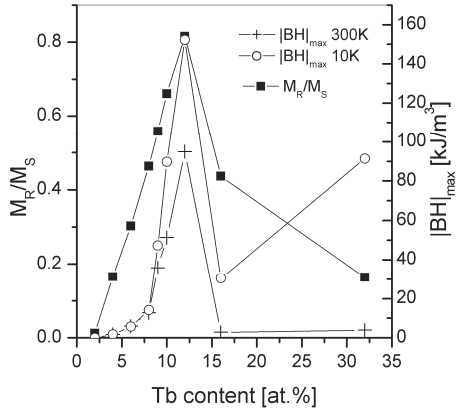

Fig. 55. M_R/M_S and $|BH|_{max}$ determined at 300 K and 10 K for $Fe_{80}Nb_6B_{14})_{1-x}Tb_x$ bulk nanocrystalline alloys

The observed changes of the parameters are obviously attributed to the variation of the magnetic phases (see Fig. 52). Due to antiferromagnetic coupling of Tb and Fe magnetic moments saturation magnetization shows a minimum at about 11 at.% of Tb. This means that for $x < 0.11$ Fe magnetic moments are dominant and for $x > 0.11$ the situation is reverse. Around this point one can observed a significant magnetic hardening i.e. maxima of H_C, M_R/M_S and $|BH|_{max}$. In the sense of hard magnetic properties, the optimize structure occurs when the balance between the phases is: 73% of $Tb_2Fe_{14}B$, 15% of Tb_2Fe and 12% of paramagnetic Fe.

As it was mentioned, one can expect some interactions between the formed phases. Such interactions of grains that posses different magnetic properties can be analysed with the use of hysteresis loop and the so-called virgin magnetization curve. For non-interacting systems the following formula is fulfilled [98,99]:

$$M_{vir}(H)-\frac{1}{2}[M_{up}(H)+M_{down}(H)]=0 \quad (50)$$

where M_{vir}, M_{up} and M_{down} are the magnetizations (determined from hysteresis loops at the same H) of the virgin, above and below it, respectively. Fig. 56 shows a deviation of equation (50) that can be considered as a measure of the inter-grain magnetic interactions.

One can see that in the both cases the deviation appears in magnetic field up to about 4 T which suggests some interactions between magnetically hard $Tb_2Fe_{14}B$ and other relatively soft phases. It is clear that for alloy with x =0.12 the interactions are stronger than for the alloy with x = 0.1. The other possibility of the origin of the "asymmetric" hysteresis loops (or deviation of eq. (50)) are blocking effects caused by a local magnetocrystalline anisotropy as well as structural disorder introduced by sample fabrication technique.

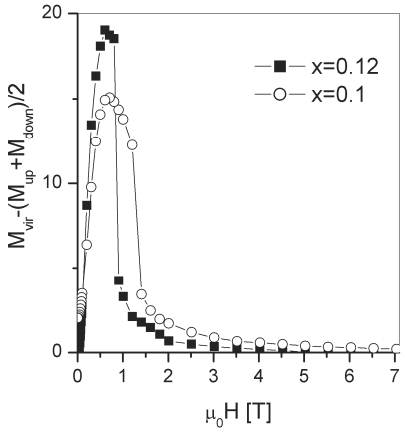

Fig. 56. Deviation of equation (50) for the alloys with x = 0.1 and x = 0.12

The T-dependent coercivity reveals some blocking and thermal activated effects. Therefore, one can expect an appearing of the time dependent magnetization or relaxation effects. Fig. 57 shows $M(t)$ curves measured after switching external magnetic field to a value $+H$, the samples had been saturated in $\mu_0 H$ = -7 T. The measurements were performed at 250 K and 300 K. The obtained results reveal a strong dependence of the relaxation effect on H, T as well as Tb content. For the sample with 8 at. % of Tb in H=0, the intensity of remanence relaxation is very weak (less than 0.1%) and increases with increasing field (for $\mu_0 H$ = 1 T it is 0.5% at 250 K and 0.55% at 300 K).

For the alloy with 16 at.% of Tb in H=0 T the relaxation intensity is much higher (2% at 250K, 1.5% at 300 K) and reveals a maximum in $\mu_0 H$=0.1 T (close to its coercive field) equal to 2.2% at 250 K and 3% at 300 K. The low intensity of remanence relaxation (H=0 T) for x = 0.08 can be explained by taking into account that this material is magnetically hard. Magnetic moments are "trapped" in energetic caves and therefore, a change of their direction requires more energy (the so-called activation one) which take place when H>0.

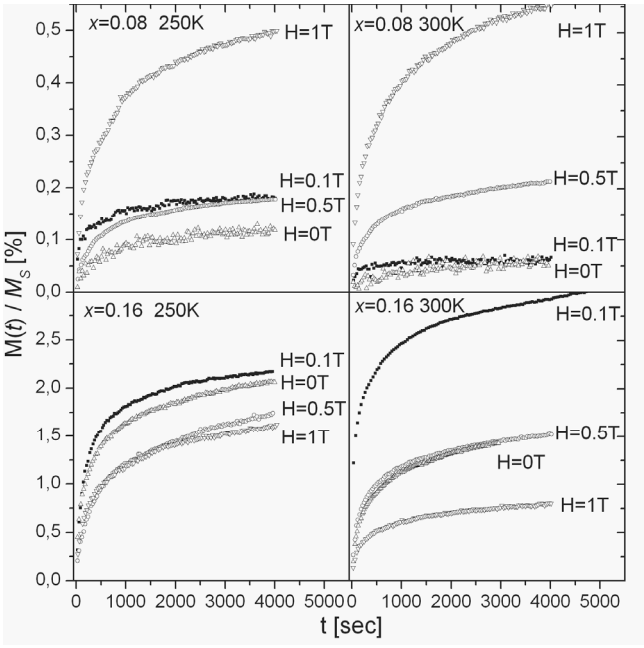

Fig. 57. M(t) curves for $(Fe_{80}Nb_6B_{14})_{1-x}Tb_x$ (x=0.08, 0.16) bulk nanocrystalline alloys (see the text)

The observed $M(t)$ dependences are not exponential and therefore, a distribution of objects with different relaxation times τ is expected to be present Similarly to the Langevin granulometry method one can determine the distribution based on the experimental $M(t)$ curves [100]. In order to analyze the relaxation times, the SA procedure was used (Sections 2.1. and 2.3). The changes in relaxation dynamics allows obtaining distribution of τ that can give more information about magnetization process. The SA procedure requires determination of saturation of the relaxation so, unsaturated components (if exist) were subtracted. The M(t) curves were analysed in H=0 (remamence relaxation) and $H \approx H_C$. It is worth to mention that in the case of the alloy with x=0.08 and H=0 the intensity of the observed effect is to weak to be analysed. The results are shown in Fig. 58. One can see two or three well separated components with Gaussian-like shapes. For the alloy with x=0.08 the change of temperature do not causes significant change of τ distribution but the contribution of objects with $\tau \approx$ 800 s is higher at T = 250 K. For the alloy with x=0.16 one can observe a shift of the positions of the components into lower τ with increase of H or T. The first components with the lowest τ are surely responsible for the observed rapid change of magnetization just after the change of magnetic field. The others components with higher τ are a picture of magnetic domains that are characterized by higher activation energy. In order to inverse direction of their magnetization it is necessary to apply higher magnetic field or higher temperature that is reflected in the observed τ distribution shift.

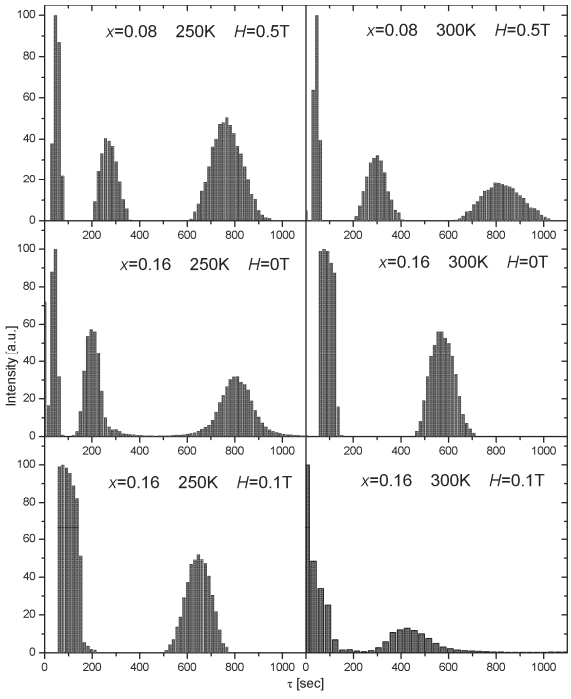

Fig. 58. The distribution of the time relaxation τ for $(Fe_{80}Nb_6B_{14})_{1-x}Tb_x$ (x=0.08, 0.16) alloys at 250 K and 300 K in different H

4.4. Gd/Ni nanoparticles

A good example of materials that reveal micromagnetic properties is Gd powder chemically coated by Ni layer (denoted as Gd/Ni). This type of powder has potential applications from at least two reasons. On one hand Gd element possesses relatively high localized magnetic moment ($7\mu_B$) and is frequently used as a magnetic addition in different nanocomposites or as a magnetic marker in different biological systems. On the other hand because of very high Gd reactivity many applications are effectively impeded or even excluded and Gd/Ni nanoparticles seem to be a solution of this problem.

The Gd/Ni powder preparation procedure consists of two stages: i) in order to obtain Gd nanopowder the commercially available Gd powder was milled for 3 h (in DMF (Dimetyloformamid) bath to prevent a possible oxidation) and ii) Gd nanopowder was nickel-plating at temperature 323 K via the chemical reaction in the following bath (pH=7): $C_4H_6O_4Ni\ 4H_2O$ (4g/100 ml) + $C_6H_8O_7\ H_2O$ (3g/100 ml) + Na_2CO_3(3g/100 ml) + NaF(0.5g/100 ml) + $NaH_2PO_2\ H_2O$(3g/100 ml) + CH_4N_2S(1g/100 ml).

Structural examinations of the obtained Gd/Ni nanopowder were carried out by applying high resolution transmission electron microscopy, as shown in Fig. 59. The micrograph reveals that diameters of the obtained Gd/Ni particles are in the range of 100 - 500 nm. Moreover in the bigger particles the higher Ni content was detected (see the EDS spectra). Magnetic properties of the powder were studied by low temperature measurements of $M(T)$ and $M(H)$. The results are briefly shown in Fig. 60.

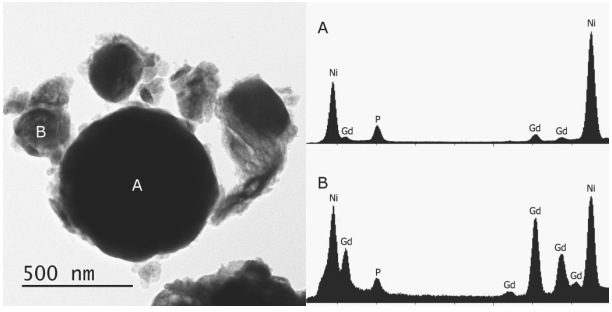

Fig. 59. TEM micrograph (on the left) and EDS spectrum (on the right) obtained in A and B area for milled and chemically nickled Gd powder

As we can see, the $M(T)$ curves measured in $\mu_0 H$ = 0.5 T result from at least the two magnetic phases: a ferromagnetic one with T_C = 290 K, and a paramagnetic one at lower temperatures. The determined value of T_C confirms that the ferromagnetic component is related to metallic Gd.

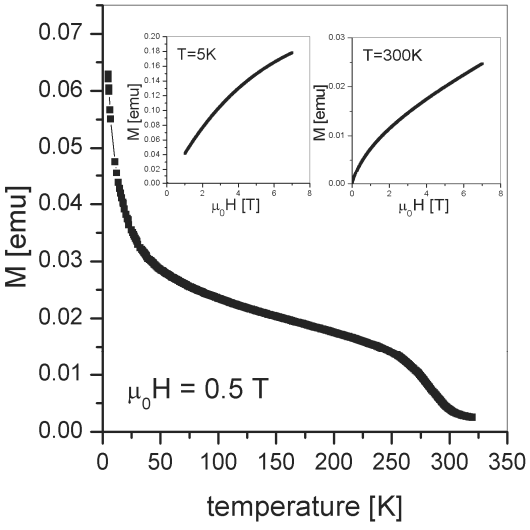

Fig. 60. Magnetic moment versus temperature for the Gd/Ni nanopowder

An origin of the paramagnetic contribution was examined by making use of the Langevin glanulometry (SA procedure) for $M(H)$ magnetic isotherms obtained at T = 5 K (after subtracting the ferromagnetic component).The result of this analysis (see Fig. 61) reveal the narrow magnetic moments distribution positioned at 6 μ_B (from 4 μ_B to about 10 μ_B), which is close to the value of free Gd atom. Therefore, the paramagnetic phase is a Gd compound (not metallic) probably Gd-O or Gd-F introduced by the preparation procedure. One can also obtain a picture of ferromagnetic Gd/Ni particles by applying the same SA method but for $M(H)$ determined at T = 100 K after subtracting of the paramagnetic (nonsaturated) component (see Fig. 62). As shown, the obtained distribution of magnetic moments id broad up to 3000 μ_B.

This example also confirms highly usefulness of the SA Langevin granulometry analysis for magnetic powder characterization.

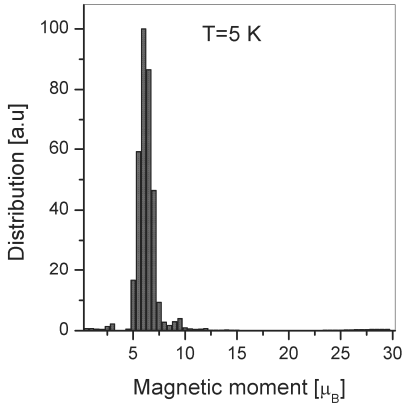

Fig. 61. Distribution of magnetic moments determined at 2 K for the Gd/Ni powder

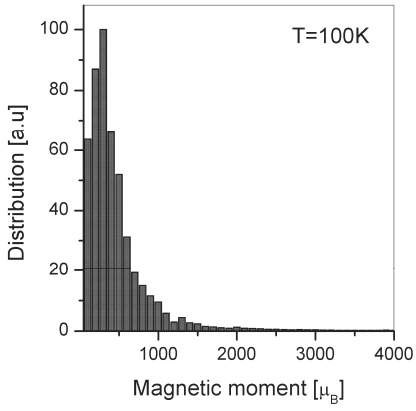

Fig. 62. Distribution of magnetic moments determined at 2 K for the Gd/Ni powder

5. Concluding remarks

As it was shown, many kind of materials reveal some attributes of the disorder in different stages including atomic disorder, interactions disorder, anisotropy disorder in the both atomic and cluster levels. Moreover, for one material a contribution of different mechanisms of the disorder is usually observed. Therefore, it is of great importance to know how an individual factor influences magnetic properties. This review present the basic phenomena of low-dimensional systems especially for magnetic nanoparticles that are widely studied in thin layers, sintered of powders magnets or in nanocomposites. According to the disordered materials, one can indicate the main three models i.e. random field, random bond and random anisotropy. Analysis of results obtaining in the frame of the models allows correctly interpreting magnetic characteristics of different modern materials such as amorphous and nanocrystalline alloys, diluted magnetics, nanocomposites or powders systems. Furthermore, the presented theory can draw a line to controlling magnetic properties of the materials in order to optimize them for different specific applications. The presented models of magnetic disorder predict the influence of nanostructure on magnetic properties which is important in technologies requiring extremely soft or hard magnets. A proper alloy composition and preparation technology allows enhanced either soft or hard magnetic properties dependently on a kind of nanostructure and introduced disorder. It was also shown, based on different examples of materials, that numerical methods concerns the elements of micromagnetism (determination of magnetic moments and relaxation time distribution) are very usefulness for wide magnetic characterization in materials science.

Acknowledgements

This work was partially supported by the Polish Ministry of Science and Higher Education under grant NN507 317336.

References

[1] M.E. McHenry, M.A. Willard, D.E. Laughin, Amorphous and nanocrystalline materials for applications as soft magnets, Progress in Materials Science 44 (1999) 291.
[2] K.H.J. Buschow , F.R. de Boer, Physics of magnetism and magnetic materials, Kluwer Academic Publishers, 2004.
[3] R. Zallen, Physics of amorphous solids, PWN, Warsaw, 1994 (in Polish).
[4] I.M.L. Billas, J.A. Becker, A. Chatelain et al., Magnetic moments of iron clusters with 25 to 700 atoms and their dependence on temperature, Physical Review Letters 71 (1993) 1067-1070.
[5] A. Hirt, D.Gerion, I.M.L. Billas et al., Thermal properties of ferromagnetic clusters, Zeitschrift für Physik D 40 (1997) 160-163.
[6] M. Getzlaff, Fundamentals of magnetism, Springer-Verlag Berlin Heidelberg, 2008.
[7] F.J.A den Braoden, W. Howing, P.J.H. Bloemen, Magnetic anisotropy of multilayers, Journal of Magnetism and Magnetic Materials 93 (2002) 562-570.
[8] A.P. Guimarães, Principles of nanomagnetism, Springer-Verlag Berlin Heidelberg, 2009.
[9] A. K´akay, M.W. Gutowski, L. Takacs, V. Franco and L.K. Varga, Langevin granulometry of the particle size distribution, Journal of Physics A, Mathematical and General 37 (2004) 6027-6041.
[10] A. Chrobak, G. Haneczok, G. Chełkowska, A. Kassiba, G. Ziółkowski, Numerical analysis of superparamagnetic clusters, Physica Status Solidi 208/11 (2011) 2692-2698.
[11] E.C. Stoner, E.P. Wohlfarth, A mechanism of magnetic hysteresis in heterogeneous alloys, Philosophical Transactions of the Royal Society A 240 (1948) 599-642, Reprinted in IEEE Transactions on Magnetism 27 (1991) 3475-3518.

[12] C. Tannous, J. Gierałtowski, The Stoner-Wohlfarth model of ferromagnetism, European Journal of Physics 29 (2008) 475-487.
[13] R Street, J.C. Woolley, A study of magnetic viscosity, proceedings of the physical society A 62 (1949) 562-572.
[14] N.T. Gorham, R.C. Woodward, T.G.St. Pierre, B.D. Terris, S. Sun, Apparent magnetic energybarrier distribution in FePt nanoparticles, Journal of Magnetism and Magnetic Materials 295 (2005) 174-176.
[15] T.G. St. Pierre, N.T. Gorham, P.D. Allen, Apparent magnetic energy-barrier distribution in horse-spleen ferritin, Evidence for multiple interacting magnetic entities per ferrihydrite nanoparticle, Physical Review B 65 (2002) 1-7.
[16] G. Haneczok, Migrational relaxation in solids, University of Silesia Publishing House, Katowice, 2011 (in Polish).
[17] Y. Imry, S.K. Ma, Random-field instability of the ordered state of continuous symmetry, Physical Review Letters 35 (1975) 1399-1401.
[18] T. Nattermann, P. Rujan, Random field and other systems dominated by disorder fluctuations, International Journal of Modern Physics B 3 (1989) 1597.
[19] D.S. Fisher, G.M. Grinstein, A.Khurana, Theory of random magnets, Physics Today 41 (1988) 56-67.
[20] S.F. Edwardst, P.W. Anderson, Theory of spin glasses, Journal of Physics F, Metal Physics 5 (1975) 965-974.
[21] S.F. Edwardst, P.W. Anderson, Theory of spin glasses II, Journal of Physics F, Metal Physics 6 (1976) 1927-1937.
[22] J.A. Mydosh, Disordered magnetism and spin glasses, Journal of Magnetism and Magnetic Materials 157/158 (1996) 606-610.
[23] A.F.J. Margownik, J.A. Mydosh, High-temperature susceptibility of the CuMn spin-glass, Physical Review B 24/9 (1981) 5277-5283.
[24] A.F.J. Margownik, J.A. Mydosh, Analysis of the high-temperature spin-glass susceptibility: Determination of the local magnetic exchange, Solid State Communication 47/5 (1983) 321-324.
[25] G.E. Brodale, R.A. Fisher, W.E. Fogle, N.E. Philips, J. Curen, The effect of spin-glass ordering on the specific heat of CuMn, Journal of Magnetism and Magnetic Materials 31 (1983) 1331-1333.
[26] V. Cannella, J.A. Mydosh, Magnetic ordering in gold-iron alloys, Physical Review B 6/11 (1972) 4220-4237.
[27] D. Hüsler, L.E. Wanger, A.J. van Duyneveldt, J.A. Mydosh, Dynamical behavior of the susceptibility around the freezing temperature in (Eu,Sr)S, Physical Review B 27/5 (1983) 3100-3103.
[28] C. Dekker, A.F. Arts, H. Wijn, Static critical behavior of the two-dimensional Ising spin glass $Rb_2Cu_{1-x}Co_xF_4$, Physical Review B 38 (1988) 8985-8991.
[29] K. Gunnarsson, P. Svendlindh, P. Norblad, L. Lungren, H. Aruga, A. Ito, Static scaling in a short-range Ising spin glass, Physical Review B 43 (1991) 8199-8203.
[30] J.A. Mydosh, Spin glasses: an experimental introduction, Taylor & Francis, Washington DC, 1993.
[31] K.H. Ficher, Spin glasses I, Physica Status Solidi B 116/2 (1983) 357-683.
[32] K.H. Ficher, Spin glasses II, Physica Status Solidi B 130/1 (1985) 13-71.
[33] T. Schneider, E. Pyttee, Random-field instability in ferromagnetic state, Physical Review 15 (1977) 1519-1522.
[34] S. Kirkpatrick, D. Shcrrington, Infinite-ranged models of sinn-glasses, Physical Review B 17 (1978) 4384-4403.
[35] J.R.L de Almeida, D.J Thouless, Stability of the Sherrington-Kirkpatrick solution of a spin glass model, Journal of Physics A 11/5 (1978) 983-990.
[36] A. Blandin, M. Gabay, T. Garel, On the mean-field theory of spin glasses, Journal of Physics C 13/3 (1980) 403-418.
[37] A.J. Bray, M.A. Moore, Metastable states in the solvable spin glass model, Journal of Physics A 14 (1981) L377-L383.
[38] D.J. Thouless, J.R.L de Almeida, J.M. Kosterlitz, Stability and Susceptibility in Parisi's solution of a spin glass model, Journal of Physics C 13/17 (1980) 3271-3280.
[39] G. Parisi, The magnetic properties of the Sherrington-Kirkpatrick model for spin glasses, Theory versus Monte Carlo simulations, Philosophical Magazine B 41/6 (1980) 677-680.
[40] D.J Thouless, P. Anderson, R.G. Palmer, Solution of 'Solvable model of a spin glass', Philosophical Magazine 35 (1977) 593-601.
[41] R. Alben, J.J. Becker, M.C. Chi, Random anisotropy in amorphous ferromagnets, Journal of applied Physics 49 (1978) 1653-1659.
[42] J.D. Patterson, G.R. Gruzalski, D.J. Sellmyer, Effect of random anisotropy on magnetic properties of amorphous systems, Physical Review B 18 (1978) 1377-1390.
[43] C. Jayaprakash, S. Kirkpatrick, Random anisotropy models in the Ising limit, Physical Review B 21 (1980) 4072-4083.
[44] A. Brooks Harris, R.G. Caflisch, J.R. Banavar, Random-anisotropy-axis magnet with infinite anisotropy, Physical Review B 35 (1987) 4929-4934.
[45] B Derridaj, J. Vannimenus, The random anisotropy axis model in the infinite-range limit, Journal of Physics C, Solid State Physics 13/17 (1980) 3261-3269.
[46] W.M. Saslow, N.C. Koon, Random-anisotropy model: Monotonic dependence of the coercive field on D/J, Physical Review B 49 (1994) 3386-3390.
[47] G. Herzer, The random anisotropy model, NATO Science Series II, Mathematics, Physics and Chemistry 184, Kluwer Academic, Dordrecht, 2005.
[48] G. Herzer, Anisotropies in soft magnetic nanocrystalline alloys, Journal of Magnetism and Magnetic Materials 294 (2005) 99-106.
[49] G. Herzer, Nano krystalline soft magnetic materials, Physica Scripta T 49 (1993) 307-314.
[50] T. Bitoh, A. Makino, A. Inoue, T. Masumoto, Random anisotropy model for nanocrystalline soft magnetic alloys with grain-size distribution, Materials Transactions 44/10 (2003) 2011-2019.
[51] B. Janus, M.S. Bucko, A. Chrobak, J. Wasilewski, M. Zych, Magnetic characterization of human blood in the atherosclerotic process in coronary arterie, Journal of Magnetism and Magnetic Materials 323 (2011) 479-48.
[52] A. Chrobak, B. Kotur, T. Mika, G. Haneczok, Effect of Gd and Fe doping on magnetic properties of $Al_{87}Y_5Ni_8$ amorphous alloy, Journal of Magnetism and Magnetic Materials 321 (2009) 2767-2771.

[53] A. Chrobak, A. Slebarski, G. Haneczok, B. Kotur, Spin-glass-like behavior and related properties of aluminum-based Al-Y-RE-Ni (RE=Gd, Dy) amorphous alloys, Journal of applied Physics 110 (2011) 113908.
[54] Proceedings of the 15th International Conference on "Soft Magnetic Materials" SMM15, Bilbao, 2003, Journal of Magnetism and Magnetic Materials 254-255 (2003) v-vii.
[55] Proceedings of the 14th International Conference on "Soft Magnetic Materials" SMM14, Budapest, 2000, Journal of Magnetism and Magnetic Materials 216-216 (2000) v-vii.
[56] Proceedings of the 14th International Conference on "Soft Magnetic Materials" SMM13, Grenoble, 1998, Journal of Physics IV/8 (1998).
[57] Current Trends in Nanoscience - From Materials to Application Proceedings of Symposium A, E-MRS Spring Meeting, Strasbourg, 2003, Materials Science and Engineering C 23, 2003.
[58] J. Rasek, Diffusion phenomena in amorphous and crystalline materials, University of Silesia Publishing House, Katowice, 2000 (in Polish).
[59] T. Kulik, Nanocrystalline soft magnetic materials obtained by the crystallisation of metallic glasses, Scientific Papers of the Warsaw University of Technology, Warsaw, 1998 (in Polish).
[60] L.K. Varga, F. Mazaleyrat, Gy. Kovács, A. Kákay, The role of the residual amorphous matrix in determining the temperature dependence of soft magnetic properties of nc alloys, Journal of Magnetism and Magnetic Materials 226-230 (2001) 1550-1552.
[61] L.K. Varga, Zs. Gercsi, Gy. Kovács, A. Kákay, F. Mazaleyrat, Stress-induced magnetic anisotropy in nanocrystalline alloys, Journal of Magnetism and Magnetic Materials 254-255 (2003) 477-479.
[62] W. Qin, Y.F. Zhang, Y.W. Du, F. Xu, Y.J. Wu, M. Zhao, F. Ma, Permeability-frequency spectra of Nanoperm alloys under different heat treatment conditions, Journal of Magnetism and Magnetic Materials 270/1-2 (2004) 174-181.
[63] W. Qin, K. Pen, W.L. Gao, F. Xu, G. Ni, Y.W. Du, Effect of cooling rate on dynamic magnetization of $Fe_{86}Zr_7B_6Cu$ nanocrystalline alloy, Materials Research Bulletin 37/8 (2002) 1393-1399.
[64] M.N. Gona, S. Yanase, S. Hashi, Y.J. Okazaki, Magnetoimpedance effect in nanocrystalline FeZrNbB ribbons, Journal of Magnetism and Magnetic Materials 254-255 (2003) 466-468.
[65] M. Miglierini, M. Seberíni, I. Tóth, K. Vitázek, Journal of Magnetism and Magnetic Materials 265/3 (2003) 243-247.
[66] G. Haneczok, P. Kwapuliński, Z. Stokłosa, J. Rasek, R. Wroczyński, Magnetic properties of nanoperm type alloys and their application on electromagnetic shields, Archives of Materials Science 24/4 (2003) 373-391.
[67] T. Gloriant, S. Suriñach, M.D. Baró, Stability and crystallization of Fe-Co-Nb-B amorphous alloys, Journal of Noncrystalline Solids 333/3 (2004) 320-326.
[68] J.E. May, M.F. de Oliveira, S.E. Kuri, The effect of Nb substitution for Zr in soft magnetic FeCoZrCuB alloy, Journal of Alloys and Compounds 369/1-2 (2004) 121-124.
[69] J.E. May, M.F. de Oliveira, S.E. Kuri, New highly magnetic and oxidation-resistant FeCo-based alloys, Materials Science and Engineering A 361/1-2 (2003) 179-184.
[70] J.S. Blázquez, V. Franco, C.F. Conde, A. Conde, Microstructure and magnetic properties of $Fe_{78-x}Co_xNb_6B_{15}Cu_1$ (x=18, 39, 60) alloys, Journal of Magnetism and Magnetic Materials 254-255 (2003) 460-462.
[71] H. Matyja, T. Kulik, Trends in non crystalline solids, World Scientufic Publishing Co, Singapore,1992, 107.
[72] Y. Hirotsu, D.E. Laughlin, G. Bertero, G. Herzer, K. Hono, Preface, Preface, Scripta Materialia 48/7 (2003) 831.
[73] H. Gleiter, Nanostructured materials: basic concepts and microstructure, Acta Materialia 48/1 (2000) 1-29.
[74] G. Haneczok, J. Rasek, Free Volume diffusion and optimisation of soft magnetic properties in amorphous alloys based on iron, Defect and Diffusion Forum 224-225 (2004) 13-26.
[75] T. Kulik, Nanocrystallization of metallic glasses, Journal of Noncrystalline Solids 287 (2001) 145-161.
[76] M.E. McHenry, D.E. Laughlin, Nano-scale materials development for future magnetic applications, Acta Materialia 48 (2000) 223-238.
[77] A. Chrobak, PhD dissertation, Optimization of soft magnetic properties in nanoperm type alloys, Silesian University, 2004 (in Polish).
[78] T. Naohara, Ageing-induced soft magnetic properties of an amorphous Fe-Si-B-Nb alloy, Philosophical Magazine Letters 78 (1998) 229-234.
[79] A. Chrobak, D. Chrobak, G. Haneczok, P. Kwapulinski, Z. Kwolek, M. Karolus, Influence of Nb on the first stage of crystallization in the $Fe_{86-x}Nb_xB_{14}$ amorphous alloys, Materials Science and Engineering A 382 (2004) 401-406.
[80] G. Haneczok, A. Chrobak, P. Kwapuliński, Z. Stokłosa, J. Rasek, N. Wójcik, Optimisation of soft magnetic properties in the $Fe_{86-x}Nb_xB_{14}$ amorphous alloys, Proceedings of the International Conference on "Soft Magnetic Materials" SMM16, Düsseldorf, 2003, 603-608.
[81] G. Haneczok, J.E. Frąckowiak, A. Chrobak, P. Kwapuliński, J. Rasek, Magnetic permeability enhancement effect in the $Fe_{86-x}Nb_xB_{14}$ (x=5, 6) amorphous alloys, Physica Status Solidi A 202 (2005) 2574-2581.
[82] A. Chrobak, M. Kubisztal, G. Haneczok, D. Chrobak, P. Kwapuliński, Z. Stokłosa, J. Rasek, Phase stability and structural relaxation in Fe-Nb-B amorphous alloys, Archives of Metallurgy and Materials 51 (2006) 561-564.
[83] A. Chrobak, G. Haneczok, D. Chrobak, Ł. Madej, G. Chełkowska, M. Kulpa, Studies of the relaxed amorphous phase in the $Fe_{80}Nb_6B_{14}$ alloy, Journal of Magnetism and Magnetic Materials 320 (2008) 770-773.
[84] Ł. Madej, G. Haneczok, A. Chrobak, P. Kwapuliński, Z. Stokłosa, J. Rasek, Long term stability of soft magnetic properties of amorphous and nanocrystalline alloys based on iron, Journal of Magnetism and Magnetic Materials 320 (2008) 774-777.
[85] A. Chrobak, G. Chełkowska, G. Haneczok, P. Kubik, Ł. Madej, Application of the coupling model to magnetic after effects in the $Fe_{72}Co_{10}Nb_6B_{12}$ amorphous alloy, Acta Physica Polonica A 115 (2009) 396-398.
[86] A. Chrobak, G. Haneczok, G. Chełkowska, Ł. Madej , Effect of structural disorder on magnetic frustrations in the $Fe_{80}Nb_6B_{14}$ amorphous alloy, Journal of Magnetism and Magnetic Materials 322 (2010) 1105-1108.

[87] G. Haneczok, Ł. Madej, A. Chrobak, P. Kwapuliński, Z. Stokłosa, J. Rasek, Influence of structural relaxation on magnetostriction in amorphous alloys based on iron, Physica Scripta 81 (2010) 025702.
[88] G. Haneczok, J. Rasek, Free volume diffusion and optimisation of soft magnetic propertiesin amorphous alloys based on iron, Defect and Diffusion Forum 224-225 (2004) 13-26.
[89] A. Chrobak, V. Nosenko, G. Haneczok, L. Boichyshyn, B. Kotur, A. Bajorek, O. Zivotsky, A. Hendrych, Effect of rare earth additions on magnetic properties of $Fe_{82}Nb_2B_{14}RE_2$ (RE = Y, Gd, Tb and Dy) amorphous alloys, Materials Chemistry and Physics 130 (2011) 603- 608.
[90] Ł. Madej, G. Haneczok, A. Chrobak, P. Kwapuliński, Z. Stokłosa, J. Rasek, Long term stability of soft magnetic properties of amorphous and nanocrystalline alloys based on iron, Journal of Magnetism and Magnetic Materials 320 (2008) 774-777.
[91] H. Kronmüller, Micromagnetism of hard magnetic nanocrystalline materials, Nanostructured Materials 6 (1995) 157-168.
[92] N. Randrianantoandro, A.D. Crisan, O. Crisan, J. Marcin, J. Kovac, J. Hanko, J.M. Grenèche, P. Svec, A. Chrobak, I. Skorvanek, The influence of microstructure on magnetic properties of nanocrystalline Fe-Pt-Nb-B permanent magnet ribbons, Journal of Applied Physics 108 (2010) 093910.
[93] M. Sagawa, S. Fujimura, H.i Yamamoto, Y. Matsuura, Permanent magnet materials based on the rare earth-iron-boron tetragonal compounds, IEEE Transactions on Magnetism 20/5 (1984) 1584-1589.
[94] A. Chrobak, M. Karolus, G. Haneczok, Preparation of Fe-based bulk amorphous and nanocrystalline alloys by mould suction casting technique, Solid State Phenomena 163 (2010) 233-238
[95] A. Chrobak, G. Haneczok, G. Chełkowska, A. Bajorek, J. Kansy, A. Hanc, Magnetic properties of Fe-Nb-B-Re (Re=Y, Gd) bulk nanocrystalline alloys, Solid State Phenomena 170 (2011) 114-117.
[96] G. Ziółkowski, N. Randrianantoandro, A. Chrobak, J. Klimontko, M. Kądziołka-Gaweł, G. Haneczok, Influence of transition and rare earth elements on magnetic properties of Fe-Nb-B-M (M=Ni, Ag, Gd, Tb) bulk nanocrystalline alloys, Acta Physica Polonica A 121/5-6 (2012) 1266-1269.
[97] A. Chrobak G. Ziółkowski, N. Randrianantoandro, J. Klimontko, G. Haneczok, Journal of Alloys and Compounds, 2012, http://dx.doi.org/10.1016/j.jallcom.2012.05) (in press).
[98] S. Thamm, J. Hesse, A simple plot indicating interactions between single-domain particles, Journal of Magnetism and Magnetic Materials 154 (1996) 254-262.
[99] S. Thamm, J. Hesse, The remanence of a Stoner-Wohlfarth particle ensemble as a function of the demagnetisation process, Journal of Magnetism and Magnetic Materials 184 (1998) 245-255.
[100] G. Ziółkowski, A. Chrobak, N. Randrianantoandro, G. Chełkowska, Numerical analysis of time dependent effects in bulk nanocrystalline hard magnets, Solid State Phenomena, 2012 (in press).